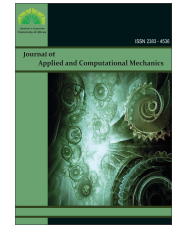




Shahid Chamran
University of Ahvaz

Journal of Applied and Computational Mechanics



Research Paper

3D Numerical Investigation of Heat Transfer Performance in Liquid-liquid Taylor Flow

MOHAMMED SAID¹, NOURA NAIT BOUDA¹, SOUAD HARMAND²

¹ Department of Energetic and Fluid Mechanics, University of Science and Technology Houari Boumediene (USTHB), P56J+GMH, Algiers, 16111, Algeria,
Email: medsaid@usthb.dz (M.S.); naitboudanora@gmail.com (N.N.B.)

² Department of Mechanics, Polytechnic University of Hauts de France (UPHF), Campus Mont Houy, Valenciennes, 59313, France, Email: Souad.Harmand@uphf.fr

Received July 29 2023; Revised October 16 2023; Accepted for publication October 17 2023.

Corresponding author: M. SAID (medsaid@usthb.dz)

© 2023 Published by Shahid Chamran University of Ahvaz

Abstract. With recent advances in semiconductor technology, conventional cooling methods and standard coolants are no longer adequate to manage electronic chips' enormous heat generation. Therefore, innovative cooling solutions are required to maintain these devices at optimum operating temperatures. Taylor flow in microchannels is an effective technique that allows excellent mixing of two fluids, which is crucial for heat transfer. A 3D numerical analysis of the heat transfer performance of liquid-liquid Taylor flow in a rectangular microchannel was carried out by ANSYS Fluent. Water droplets were dispersed in either ethylene or propylene glycol, with the interface between the two fluids captured using the Volume of Fluid method. For optimal computational time, two symmetries in the XY and XZ planes are considered. Furthermore, mesh size refinement was performed in the near-wall region to capture the liquid film. An analysis of the effect of plug/slug length and liquid film thickness is conducted with initially constant thermo-physical properties. This assumption was considered to analyse the heat transfer process and determine the most critical parameter affecting heat transfer performance. A user-defined function is then implemented in ANSYS Fluent to examine the effect of working fluids temperature-dependent viscosity change on the heat transfer rate. Conjugate heat transfer and axial conduction are also examined, as these two factors can significantly affect the thermal behaviour inside the microchannel and enable the achievement of realistic and accurate results. The results reveal that Taylor liquid-liquid flow can increase the heat transfer rate by up to 440% over single-phase flow. It was also found that the temperature-dependent viscosity of the working fluids significantly affects the plug/slug length and liquid film thickness, resulting in a 20.8% improvement in heat transfer rate compared with constant thermo-physical properties. This study will improve the state of knowledge on heat transfer by Taylor flow in microchannels and factors that can influence it, and highlight the significance of this flow pattern in enhancing heat transfer performance over single-phase flow.

Keywords: 3D simulation, Taylor flow, heat transfer, liquid film, microchannel.

1. Introduction

In today's modern world, microelectronics is part of all aspects of human life. It can be found in our daily lives as consumers (personal computers, mobile phones, fax machines, etc.), in the transport sector (autonomous driving, mobile communications, etc.), in the medical field (miniaturised medical devices, instruments, implants, etc.), and finally in the military and aerospace industry.

Thermal management and control of electronics devices, however, has become a challenge and a complex issue with the rapid miniaturisation and large-scale integration of electronics. One of these challenges consists of efficiently removing the large amount of heat generated by these microelectronic devices to ensure a long-life cycle.

Conventional cooling approaches (natural convection, air cooling) are becoming less and less efficient and are no longer able to remove the heat flow produced by electronic devices already exceeds 300 W/cm². This, in turn, poses a real challenge for the microelectronics industry, as the temperature of electronic devices must be kept below 85°C [1]. Therefore, new cooling techniques, mechanisms and fluids with high heat transfer capacity need to be developed in order to improve the heat removal rate to maintain their normal operating temperature.

Researchers have proposed a new innovative cooling techniques that improve the rate of heat transfer in microchannels and to provide a minimum thermal resistance and pressure drop sufficient to satisfy cooling requirements [2]. In general, these techniques can be classified into two groups: active and passive.

The active method uses external energy source, such as a microfine array to generate vibrations [3], a periodic electric field technique [4], a flow pulsation technique [5]. The passive method, on the other hand, does not require external energy and entails the use of surface roughness [6], flow disruption [7], channel curvature [8], obstruction, two-phase flow [9-11] and nanofluid [12]. It



is generally accepted that passive methods are much more popular than active methods. One reason for this is their low cost, while another is their simplicity of implementation.

We focused our attention here on the implementation of two-phase flow, precisely Taylor flow inside microchannel, as a passive and alternative method for inducing mixing and increasing heat transfer rates with reasonable pressure drop.

Many previous studies have been conducted to fully understand this kind of two-phase flow, starting with hydrodynamics [13, 14], liquid film [15, 16], pressure drop [17, 18], and even in the field of heat transfer [19, 20]. However, few experimental studies have been conducted on liquid-liquid two-phase flow associated to the heat transfer [11, 19–22].

Asthana et al. [21] conducted experiments on the liquid-liquid two-phase flow heat transfer in a six turn Serpentine microchannel with a hydraulic diameter of 100 μm . The mineral oil plugs were dispersed in a water carrier phase causing boundary layer interruptions and better mixing. The temperature distribution was obtained by the laser induced fluorescence (LIF) method, while for the velocity field, micro-particle image velocimetry (Micro-PIV) was used. It was observed that the Nu number was much more interesting (four times higher) for water-oil slug flow compared to pure water (single phase flow). However, this is associated with an increase in pressure drop compared to single phase flow.

The heat transfer of a liquid-liquid Taylor flow in a 1.5 mm circular tube was investigated experimentally by Giolla Eain et al. [11]. The experiments were conducted using a variety of carrier fluids, namely Pd5, Dodecane, and AR20 silicone oils, with water as the dispersed phase. The temperature of the heated wall was measured by high resolution infrared thermography. The researchers confirmed the report previously published by Asthana et al. [21] and stated that heat transfer can be improved by as much as 600% with two immiscible liquid phases. They also noted that the increase in the liquid film that separates the dispersed phase from the wall will negatively impact heat transfer. The impact of the length of plugs and slugs was also evaluated on heat transfer.

Dai et al. [22] studied the heat transfer characteristics of hexadecane plugs dispersed in water as a continuous phase in a vertical tube of 2 mm diameter. A constant heat flux was chosen as the thermal boundary condition on the wall. The results show that the experimental and numerical heat transfer coefficients are in good agreement. The researchers pointed out the strong dependence of the Nusselt number on experimental uncertainties in flow parameters, such as inlet flow rates, inlet fluid temperature, etc. In addition, they developed a heat transfer model involving heat transfer from the wall to a liquid film region and from the film separately to the slug and droplet. This heat transfer model was able to correlate their numerical (liquid-liquid) and experimental (gas-liquid) data with a relative standard deviation of 20%.

In order to improve the heat transfer performance, the Taylor liquid-liquid flow in a heated mini-curved tube is studied experimentally by Adrugi et al. [20]. The tube has an internal diameter of 1.65 mm. In addition, different bending radii and lengths are used in the experiments. The Taylor flow was created using water as the continuous phase and low viscosity silicone oils (0.65 cSt, 1 cSt and 3 cSt) as the dispersed phase. It was shown that the use of liquid-liquid Taylor flow in miniature-scale curved tubes improves heat transfer rates compared to single-phase flow.

An experimental and numerical study was recently conducted by Abdollahi et al. [19, 23] on Taylor liquid-liquid flow submitted to heat transfer in a rectangular microchannel with a hydraulic diameter of 2 mm. The researchers used Hexadecane, Kerosene and water as working fluid. Numerically, the authors considered only a quarter of the microchannel to minimise the computational cost. With a constant heat flux at the wall, good agreement was found between the experimental data and the numerical results. At low capillary numbers, their results showed that the Nu number was almost independent of the two-phase velocity. Furthermore, by increasing the slug length, Abdollahi et al. [19] reported a decrease in the friction factor as well as the Nu number. Finally, an improvement in heat transfer performance of 700% was reported when using two-phase flow compared to single-phase flow.

Some other researchers have numerically studied fluid flow and heat transfer in microchannels. Ubrant et al. [24] conducted a 2D axisymmetric numerical study of the heat transfer associated with a Taylor "water-oil" flow in a circular microchannel of 100 μm inner diameters. Based on the *Volume of Fluid* method (VOF), the interface of the two immiscible liquids was captured. They reported that droplet-laden flows significantly enhance the rate of heat transfer compared to conventional heat transport in a single-phase oil flow.

Another numerical study, in a two-dimensional and axisymmetric configuration, was carried out by Fischer et al. [25]. The effect of liquid/liquid Taylor flow on heat transfer in a microchannel was analysed using Silicone oil, water and polyalphaolefin "PAO" as working fluids. Taylor's "liquid/liquid" heat transfer was found to be more effective compared to single phase flow. However, the pressure drop in two-phase Taylor flow was higher than that in single phase flow. Furthermore, researchers reported that droplets with high viscosities would improve heat transfer. Besides, they concluded that adding 3% of Al_2O_3 nanoparticles to the dispersed phase did not provide much additional heat transfer enhancement (3% to 5%).

In 2012, the effect of plug length and Peclet number was examined by Che et al. [26] in a numerical two-dimensional study under a constant wall temperature boundary condition. According to the researchers, short plugs improved heat transfer in microchannels compared to long plugs. Additionally, an increase in Nusselt number was observed with a higher fluctuation when Peclet numbers were large.

Few years later, the same authors Che et al. [27] conducted a more in-depth study of heat transfer in microchannels. They performed a three-dimensional numerical study in a rectangular microchannel by dispersing water droplets in a continuous phase of mineral oil. The finite volume method was used for the flow field and heat transfer, while the level set method was used to capture the interface. In addition, a moving reference frame was used to reduce the computational time. The researchers showed that the three-dimensional structure of the flow significantly affected the heat transfer. They noted that liquids between the droplet interface and the corner of the microchannel hinder the heat transfer process due to their parallel flow. In contrast, recirculation within the droplets and in the region between successive droplets can induce significant heat transfer with a Nusselt number of 10 to 15 times greater. Effects such as droplet length, channel cross-section aspect ratio and Peclet number were investigated in this study.

Alireza et al. [28] conducted a 3D-numerical simulation in a square channel with a hydraulic diameter of 100 μm to study flow field and heat transfer liquid-liquid slug flow. A mineral oil and water were selected as working fluids and a constant wall temperature boundary condition is used. In addition to the refinement of the basic mesh at the walls, a dynamic mesh adaptation based on the gradient of volume fraction was employed in order to capture the liquid film surrounding the droplet. The authors concluded that the liquid-liquid interfaces and the curvatures of the walls increase radial velocity which in turn increases convective heat transfer. Furthermore, it has been observed that a wavy channel containing a slug flow provides the best performance.

Using a 2D numerical simulations, Vivekanand et al. [29] explored the heat transfer and flow characteristics of a Taylor mineral oil-water flow in a circular microchannel ($D = 100 \mu\text{m}$). Constant wall temperature of 373 K and constant heat flux of 420 kW/m^2 were both prescribed over the wall of the microchannel. Compared to liquid single-phase flow, the researchers observed a



significant increase in the Nusselt number, up to 180% in the case of a Dirichlet thermal condition and 210% for the Newman one. As a result, they suggested considering a constant heat flow at the wall rather than an isothermal wall.

Recently, a 2D numerical simulation is conducted by Chandrasekhar et al. [30] on the commercial software ANSYS Fluent, to study Taylor liquid-liquid flow and heat transfer in plain and wavy circular microchannels. A microchannel with a diameter of $D=100\ \mu\text{m}$ containing mineral oil droplets dispersed in a water carrier phase. An isothermal boundary condition is imposed at the wall to study the heat transfer performance. With a wavy channel, the results show that the overall Nu number can increase by up to 130% compared to a single-phase flow. Moreover, a slight increase of 6% in the Nusselt number as well as a slight increase in the pressure drop were observed compared to two-phase flow in a straight microchannel.

A two-dimensional numerical study of the heat transfer enhancement caused by two-phase droplet flow in a cylindrical microchannel of $100\ \mu\text{m}$ diameter has been carried out by Li et al. [31]. Water and oil were used as working fluids. The authors assumed water having the same properties as oil, except for its dynamic viscosity in order to eliminate any influence of the thermophysical properties of the water droplets on the heat transfer.

So, the results showed that Nu number increases significantly when droplets are dispersed in a single-phase flow with a small pressure drop. It was also found that heat transfer does not increase proportionally with increasing droplet size or flow rate. The effect of wall slip velocity in the continuous phase on heat transfer enhancement was also analysed. Researchers defined the boundary conditions for wall slip velocity using the Navier slip model as expressed below:

$$\tau_{\text{Wall}} = \mu \frac{U_s}{L_s}$$

τ_{Wall} , μ , U_s , and L_s represent the shear stress exerted by the fluid on the wall, fluid viscosity, wall slip velocity, and wall slip velocity length. By increasing L_s , the researchers observed a slight increase in the average Nu number in both single-phase and two-phase flows. This is mainly due to enhanced heat transfer in the continuous phase. However, with the increase in L_s , a slight decrease was noticed in the liquid film thickness and the average vorticity inside the droplet. This consequently weakens heat transfer in two-phase flows.

The thermal characteristics of liquid-liquid Taylor flow were studied by Chandrasekhar et al. [32] using numerical simulations in a 3D microchannel with uniform wall heat flux boundary conditions. Dodecane and water were considered respectively as primary and secondary phase. Then the effects of five different thermal boundary cases were considered, as well as the aspect ratio of microchannels to study the heat transfer characteristics. First, the results indicate that the pressure drop in the Taylor flow does not change with the thermal boundary condition in contrast to the aspect ratio Ar . Chandrasekhar et al. [32] reported that for $Ar=1$, the best thermal performance ($Nu=9.85$; $Nu=10.41$) was achieved when four walls or opposite walls were heated. However, increasing the aspect ratio ($Ar=2$; $Ar=5$) significantly reduces the heat transfer rate for almost all thermal boundary conditions studied.

In light of the numerical research available in the literature and reviewed here, most of these studies are two-dimensional and a few have been performed in 3D. Furthermore, the majority of the working fluids used in these studies are often water and oil, with constant thermophysical properties. While it is well-known that temperature can significantly affect thermophysical properties, particularly viscosity, which can greatly affect heat transfer performance. Moreover, we noticed that the majority of numerical studies in the literature were conducted in microchannels of $100\ \mu\text{m}$ width (or hydraulic diameter), and only two were conducted in microchannels of 1 and 2 mm. So, present study aims to investigate the heat transfer performance of novel working fluids in a rectangular microchannel of $300 \times 600\ \mu\text{m}^2$ cross-section. The effect of the temperature dependence of the working fluid viscosity as well as the conjugate heat transfer and axial conduction on the heat transfer performance were investigated.

2. Methodology

A three-dimensional numerical study of liquid-liquid Taylor flow associated to heat transfer in a rectangular microchannel is presented in this work. The simulations are performed under ANSYS Fluent CFD solver.

2.1. Governing equations

In this study, the Volume of Fluid method introduced by Hirt and Nichols [33] is used to capture the interface between the two liquids. We chose this method as it is computationally efficient compared to other method available in ANSYS Fluent (Coupled Level-set Volume of Fluid method CLVOF). In each control volume, the total volume fraction of all phases is equal to unity, and the interface is localised whenever the volume fraction φ in a control volume is between 0 and $1(0 < \varphi < 1)$.

The volume fraction equation with the assumption of zero mass transfer between the two phases is as follows:

$$\frac{\partial \varphi}{\partial t} + u \nabla \cdot (\varphi) = 0 \quad (1)$$

To apply "single-fluid" formulation (where a common flow field is shared for both phases), fluid properties such as density ρ , viscosity μ , and thermal conductivity k are expressed as the volume fraction weighted average between the two fluids [34]:

$$\phi = \varphi_d \phi_d + (1 - \varphi_d) \phi_c \quad (2)$$

where φ is the volume fraction and the indices d and c denote the dispersed and continuous phase, respectively.

To capture the interface of liquid-liquid Taylor flow, the conservation equations, namely mass, momentum and energy conservation, were solved simultaneously with the volume fraction advection equation (Eq. (1)). The conservation equations are presented as follows [35, 32]:

Continuity:

$$\frac{\partial \rho}{\partial t} + \nabla \cdot (\rho u) = 0 \quad (3)$$

Momentum:

$$\frac{\partial (\rho u)}{\partial t} + \nabla \cdot (\rho u u) = -\nabla p + \nabla \cdot [\mu (\nabla u + \nabla u^T)] + F \quad (4)$$



Thermal energy:

$$\frac{\partial(\rho e)}{\partial t} + \nabla \cdot (u\rho h) = \nabla \cdot (k\nabla T) \quad (5)$$

where e and h are the energy and enthalpy, respectively.

To calculate the effects of surface tension at the interface between the two liquids, the continuum surface force (CSF) model of Brackbill et al. [36] is applied. This model includes surface tension forces, represented by the term (F) in the momentum equation (Eq. (4)), as a body force acting at the liquid-liquid interface.

The body force term (F) in Eq. (4) can be written as [36]:

$$F = \sigma\kappa\delta\hat{n} \quad (6)$$

where κ is the interface curvature and is defined in terms of the divergence of the normal interface (\hat{n}):

$$\kappa = \nabla \cdot \hat{n} = \nabla \cdot \frac{\mathbf{n}}{|\mathbf{n}|} \quad (7)$$

with \mathbf{n} is the normal vector as:

$$\mathbf{n} = \nabla\varphi \quad (8)$$

2.2. Working fluids

In this study, ethylene glycol and propylene glycol were used as the continuous phase whereas water was chosen to be the dispersed phase. These cooling fluids are assumed to be Newtonian, incompressible and immiscible, and they were selected based on different criteria such as flammability, non-toxicity, cost, and availability on the market. It is worth noting that propylene glycol is less toxic than ethylene glycol. However, ethylene glycol has superior heat transfer properties due to its low viscosity compared to propylene. In Table 1, we present the properties and characteristics of the coolants also available in the literature [37-39].

2.3. Geometrical model and boundary conditions

The geometry dimensions are the same as those used in our previous work [40] as well as the experimental work of Ma et al. [16]. The schematic configuration and the channel geometry are shown in Fig. 1. It is a rectangular channel of $W = 600 \mu\text{m}$ and $h = 300 \mu\text{m}$ with a total channel length of $L = 29 \text{ mm}$ whose walls are considered to be made of aluminum.

As the fluid flow is symmetrical along the central plane of the microchannel, we considered just a quarter of the microchannel, assuming two symmetries along the XY and XZ planes. This choice aims to reduce the computational time and extend the length of the 3D microchannel a little further. The same double symmetry assumption has been used in several studies of Taylor flow in microchannels [10, 23]. In a recent study on fluid flow and heat transfer of Taylor flow in microchannels, Abdollahi et al. [23] simulated a quarter of a square microchannel and they successfully validated their numerical model against their experimental data. Based on that, we can say that the symmetry assumption does not affect the accuracy of the results for Taylor flow studies in mini and microchannels.

Table 1. Properties and characteristics of the coolants at 20 °C.

Coolant	Boiling point at 1 atm (°C)	Thermal conductivity (W/m.K)	Specific heat (kJ/kg.K)	Density (Kg/m ³)	Viscosity (mPa.s)	Surface Tension (N/m)
Water (W)	100	0.613	4.18	1000	0.89	
Ethylene glycol (EG)	198	0.26	2.84	1109	19.83	0.048
Propylene glycol (PG)	184	0.1962	2.479	1035.3	57.57	0.0716

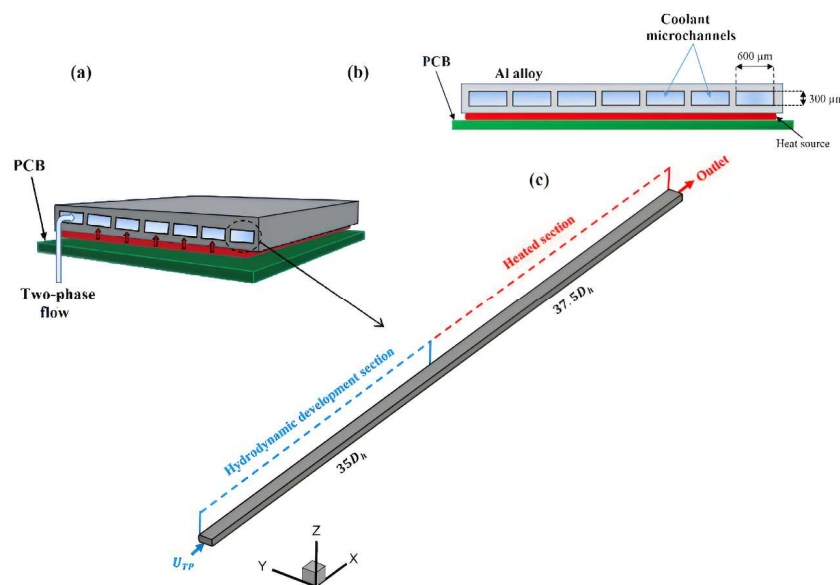


Fig. 1. Schematic design of the 3D microchannel used in this study.



Table 2. The input parameters for both methods.

	Patching method			T-junction method		
	Patch length (m)	Distance between patches (m)	Mixture velocity U_{TP} (m/s)	Continuous phase velocity U_c (m/s)	Dispersed phase velocity U_d (m/s)	Flow rate ratio q
EG/W	1.1×10^{-3}	1.445×10^{-3}	0.037	0.0185	0.0185	1
PG/W	8.4×10^{-4}	1.36×10^{-3}	0.037	0.0185	0.0185	1

In order to ensure hydrodynamic development of the plugs, a length of 14 mm ($\sim 35D_h$) is chosen for the hydrodynamic development region. In this part, the wall temperature was set equal to the temperature of the carrier phase (20 °C).

Four water patches were placed at the microchannel entrance region to create dispersed plugs in a carrier phase (propylene or ethylene glycol). The patch length and the distance between them and other parameters are shown in Table 2. These parameters were chosen so that we could ultimately obtain the same droplet and slug length generated by the T-junction method.

The water patches were placed 1 mm from the microchannel inlet. This distance, known as development length L_{dev} , is essential for inlet flow development (See Fig. 2). It is fixed according to the entrance length calculated using the correlation introduced by Dombrowski et al. [41].

Afterwards, the plugs enter the heated section ($37.5D_h$) where the flow is subjected to constant heat flow rate of 30 kW/m². A uniform velocity is maintained at the inlet, while a pressure outlet condition was set at the outlet. In order to prevent wettability effects, a 180-degree contact angle was set. Moreover, a non-slip boundary condition was applied into the channel walls. Two symmetry planes (on the XZ and XY planes) were applied to reduce the computational time cost (see Fig. 1c and Fig. 3).

2.4. Flow solver

ANSYS Fluent software which is based on the finite volume method was used to perform the simulations. An explicit geometric reconstruction approach was adopted to solve the VOF equation and ensure the sharpness of the interface. In addition, the first-order Implicit method was used to solve the transient terms of the flow equations. The QUICK method and the second-order UPWIND method were used respectively to solve the momentum and energy equations. The QUICK scheme, based on a weighted average of second-order upwind and central interpolations of the variable, provides more precise results for structured hexahedral mesh [28]. The PISO scheme was selected for the pressure-velocity coupling. To reduce the spurious currents induced by the discretization of the surface tension term [42], Green-Gauss node-based technique was used, in which the values are calculated as the arithmetic mean of values at the nodal points on the face [43]. A fixed Current number, equal to 0.25, was used in this study. This choice allows for a variable and sufficiently small time-step, which varies according to the control volume size, particularly, in the near-wall region. The resulting time steps are in the order of 10⁻⁶s. The residual for continuity equation was set to 10⁻⁴ while for the remaining variables, the residuals were kept as low as possible.

3. Results and Discussion

3.1. Mesh grid independency

The computational domain was generated and meshed using ICEM CFD. Here, we employ a non-uniform structured mesh with mesh refinement in the near-wall region. Since we have used the continuum surface force (CSF) model to calculate the effects of surface tension at the interface, it is imperative to use a structured mesh to reduce the discrepancies that may occur with the CSF method [23]. We maintain an aspect ratio of 1 (cubic meshes in 3D simulation) to prevent the generation of spurious currents and minimise uncertainties [42]. In the near-wall region, the size of the first layer along the Y and Z directions was kept constant with values equal to 5 and 3 μm , respectively, and an aspect ratio equal to 1.2 (See Fig. 3). Gupta et al. [42] have indicated that a minimum of five elements are required in the near-wall region to effectively capture the thin liquid film.

Four different mesh sizes, namely 25 μm , 17 μm , 12 μm and 7 μm , were chosen to study mesh independence. The refinement near the wall (along the y-axis and the z-axis) was kept constant for the different mesh sizes. These mesh sizes were chosen based on the computational time and the interface sharpness at the plug front and back.

A mixture velocity of $U_{TP} = 0.037$ m/s and an initial patch length of 1.1 mm for the ethylene glycol/water combination were chosen for the mesh independence study.

Figure 3 shows the mesh adopted in the XZ and YZ planes and in the near-wall region. As mentioned above, a cubic mesh was used far from the microchannel walls to minimise spurious currents. It can be also noticed that the two symmetry planes along the XY and XZ planes are included as mentioned above [42].

The comparison between these different meshes was performed in terms of the longitudinal velocity in the y and z direction (Figs. 4 and 5) normalized by the mixture velocity U_{TP} , as well as the pressure drop along the plug (See Fig. 6).

From Figs. 4. and 5, it can be seen that at the wall location, there is no significant variation among the four meshes. For the finest meshes (7.12 and 17 μm), the curves almost merge.

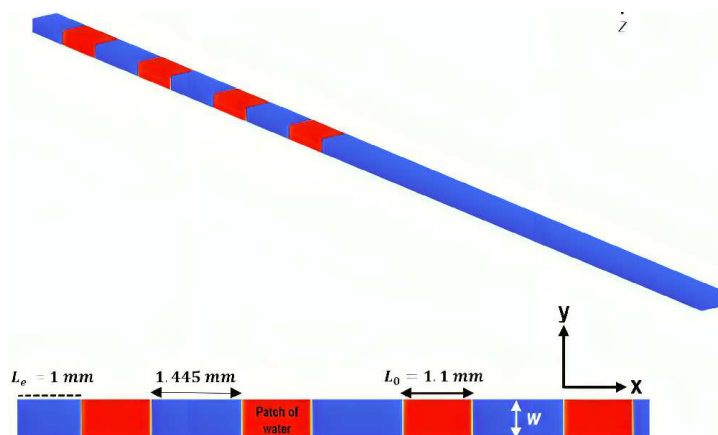


Fig. 2. The input parameters for the EG/W case using the patching method.



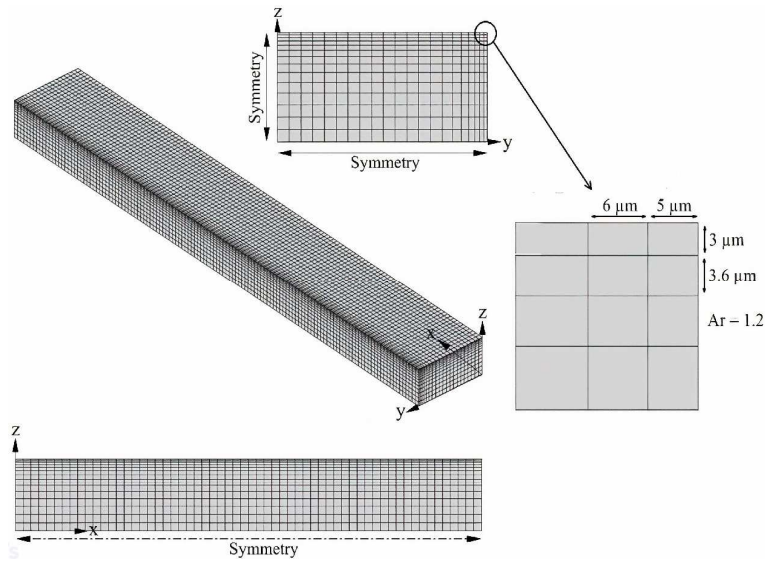


Fig. 3. The computational mesh of the 3D rectangular microchannel.

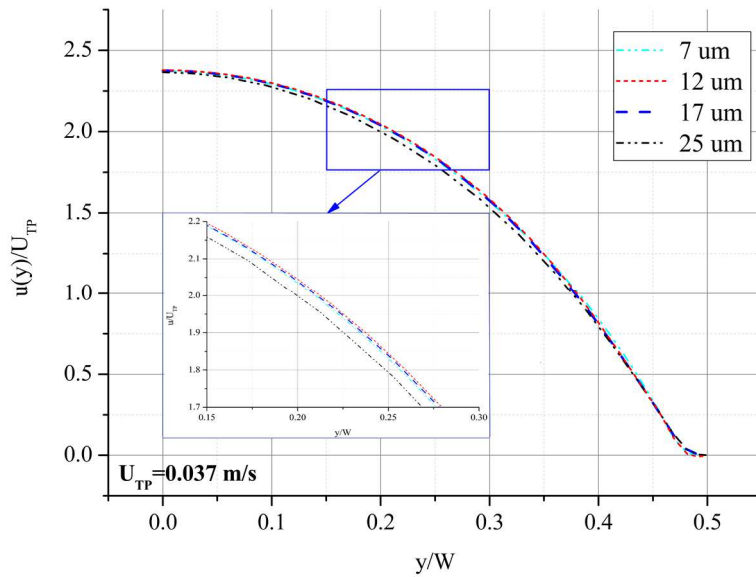


Fig. 4. The longitudinal velocity normalized by U_{TP} , along the y -direction.

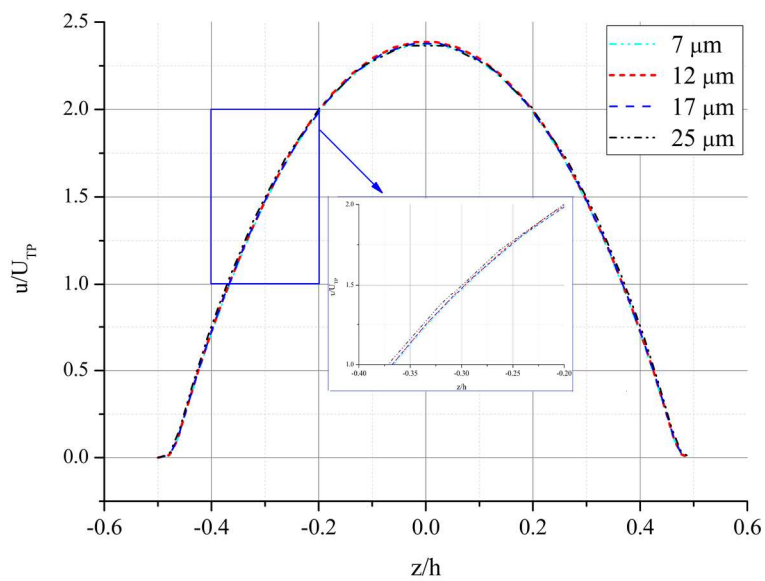


Fig. 5. The longitudinal velocity normalized by U_{TP} , along the z -direction.



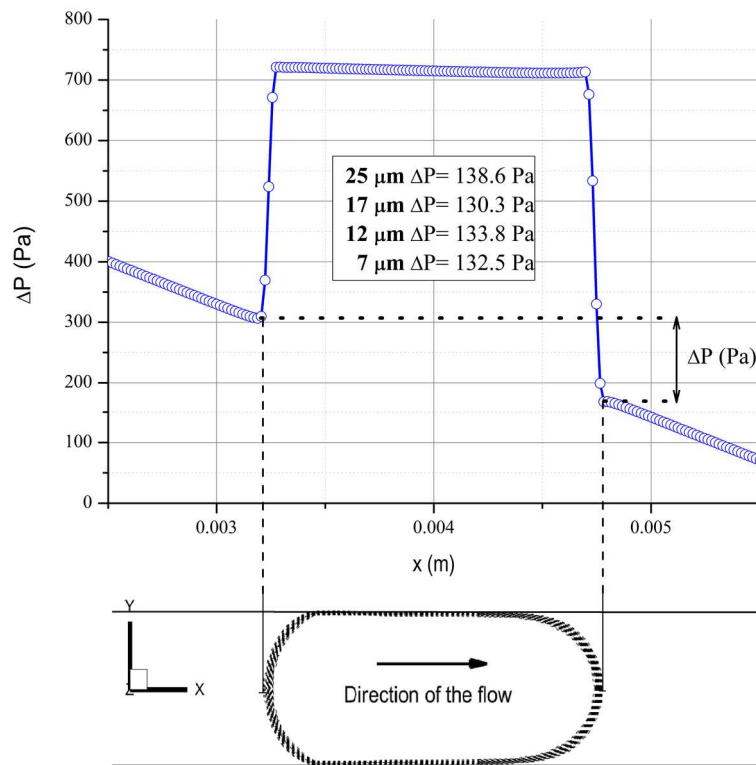


Fig. 6. The pressure drop along the plug for different mesh size.

The same observations can be made in terms of pressure drop. As can be seen in Fig. 6, all three meshes (7 μm , 12 μm and 17 μm) show almost the same pressure drop. Therefore, the simulations were carried out with a mesh size of 17 μm to save computational time, achieve a sharp interface, and achieve acceptable results.

3.2. Validation

The present study was validated by performing a comparison between the T-junction method previously validated by the experimental results of Ma et al. [16] in our previous work [40], and the patching method used in this study. The droplet/slug length, the liquid film in the corners and along the Y and Z directions, and the curvature radius of the droplet's front and back (See Table 4) are presented.

The liquid film results were also compared to the experimental correlations presented in Table 3. It should be noted here that the correlation performed by Ma et al. [16] and Yao et al. [44] was developed on a geometry that has the same dimensions as the one used in this study. However, the correlation of Ma et al. [16] was performed for predicting the liquid film in the corners (δ_{cr}) of liquid-liquid two-phase systems, in contrast to the correlation of Yao et al. [44] was performed for predicting the liquid film in the near-wall region (δ_y) of two-phase gas-liquid systems (See Table 3). We further compared the results of the liquid film in the corners with the experimental correlation developed by Kreutzer et al. [45] originally developed for gas-liquid systems in a square microchannel.

Table 3. Experimental correlations of film thickness.

Correlation	Operation conditions	Reference
$\frac{\delta_y}{W} = 0.15[1 - \exp(-8.221Ca_d^{0.972})]$	Rectangular microchannel ($0.00065 < Ca_d < 0.3$)	Yao et al. [44]
$\frac{\delta_{cr}}{W} = 0.249 - 0.182 \exp(-13.9Ca_d^{0.944} Re_{TP}^{-0.202})$	Rectangular microchannel ($0.0003 < Ca_d < 0.15$)	Ma et al. [16]
$\frac{\delta_{cr}}{W} = 0.35 - 0.25 \exp(-2.25Ca_d^{0.445})$	Square microchannel ($Ca_d < 3.0$)	Kreutzer et al. [45]

Table 4. A comparison between the T-junction and patching methods for the two chosen combinations.

Fluid combination	Method	Studied parameters					
		Droplet/slug length		Droplet shape		Film thickness	
		LD/W	LS/W	Rfront/W	Rtail/W	δ_y/W	δ_{cr}/W
EG/W	T-junction	2.35	1.76	4.05×10^{-1}	5.06×10^{-1}	0.015	0.1109
	Patching	2.43	1.68	4.13×10^{-1}	5.09×10^{-1}	0.014	0.1112
	Deviation (%)	3.4	4.5	1.9	0.6	6	0.3
PG/W	T-junction	2.08	1.53	3.63×10^{-1}	4.8×10^{-1}	0.0433	0.134
	Patching	2.07	1.48	3.7×10^{-1}	4.79×10^{-1}	0.0408	0.136
	Deviation (%)	0.5	3.2	1.9	0.2	5.7	1.5



Table 5. Measurements of the dimensionless liquid film at the corner obtained by the patching method versus experimental correlations.

Fluid combination	δ_{cr}/W				
	Patching method	Ma et al. correlation	Deviation (%)	Kreutzer et al. correlation	Deviation (%)
EG/W	0.111	0.116	4	0.118	6
PG/W	0.136	0.168	19	0.134	2

Table 6. Measurements of the dimensionless liquid film on the y-axis obtained by the patching method versus experimental correlations.

Fluid combination	δ_y/W		
	Patching method	Yao et al. correlation	Deviation (%)
EG/W	0.014	0.022	36
PG/W	0.0408	0.0426	4

Table 4 shows the results obtained for the two fluid combinations by both methods. As can be seen, although the droplet formation method differs between the two methods, the presenting results show good agreement indicating the reliability of the patching method.

Two combinations of fluids (*ethylene glycol/water* “EG/W” and *propylene glycol/water* “PG/W”) were chosen for the validation, with fluid properties and input parameters listed in Tables 1 and 2, respectively. The Ca_D number (based on droplet velocity U_D) for the EG/W and PG/W combinations is 0.037 and 0.0173, respectively, which falls into the domain of validity of the correlations previously introduced (See Table 3).

Table 5 and 6 show the dimensionless liquid film results obtained by the patching method against the experimental correlations introduced above (See Table 3).

For the liquid film in the corners δ_{cr} , the simulation results are in good accordance with the correlations introduced by Ma et al. [16], and Kreutzer et al. [45]. For the EG/W combination, the relative error between the simulation results and the correlation of Ma et al. [16] was 4%, while for the correlation of Kreutzer et al. [45], the relative error was 6%. On the other hand, for the PG/W combination, the liquid film thickness (δ_{cr}) obtained by our simulations agrees well with the correlation of Kreutzer et al. [45] with a relative error equal to 2%.

For the liquid film in the near-wall region (δ_y), the correlation of Yao et al. [44] overestimates the liquid film thickness for both fluid combinations (see Table 6). However, the relative error between our simulation results and the correlation is only 4% for the PG/W combination compared with 19% for the EG/W combination. The same observation was noted by Abdollahi et al. [19] and Ma et al. [16], who reported that for a $Ca_D < 0.03$ (based on droplet velocity U_D), the film thickness for liquid-liquid systems is always less than the correlation prediction. They explained that the superior dispersed phase viscosity of liquids compared to gases results in higher viscous shear at the plug interface in the film region, leading to a lower liquid film in liquid-liquid systems than in gas-liquid systems. It is worth mentioning that the capillary number (Ca_D) for the EG/W combination is 0.0173, while for PG/W, the Ca_D is 0.037.

Figure 7 compares the liquid film results (δ_y and δ_{cr}) obtained by the patching method with the experimental correlations and the numerical results of Said et al. [40].

For the liquid film in the corners (δ_{cr}), the simulation data from Said et al [40] and the results obtained by the patching method (the hollow squares) agree well with the correlation of Kreutzer [45] for all viscosity ratios λ , achieving an average relative error of 4%. However, for the Ma et al. [16] correlation, the numerical results deviate from the correlation at low viscosity ratios λ , with a mean relative error of 14%. Regarding the liquid film in the near-wall region, the simulation data shows the same trend and agrees well with the correlation of Yao et al. [44] for low viscosity ratio λ , with an average relative error of 17%.

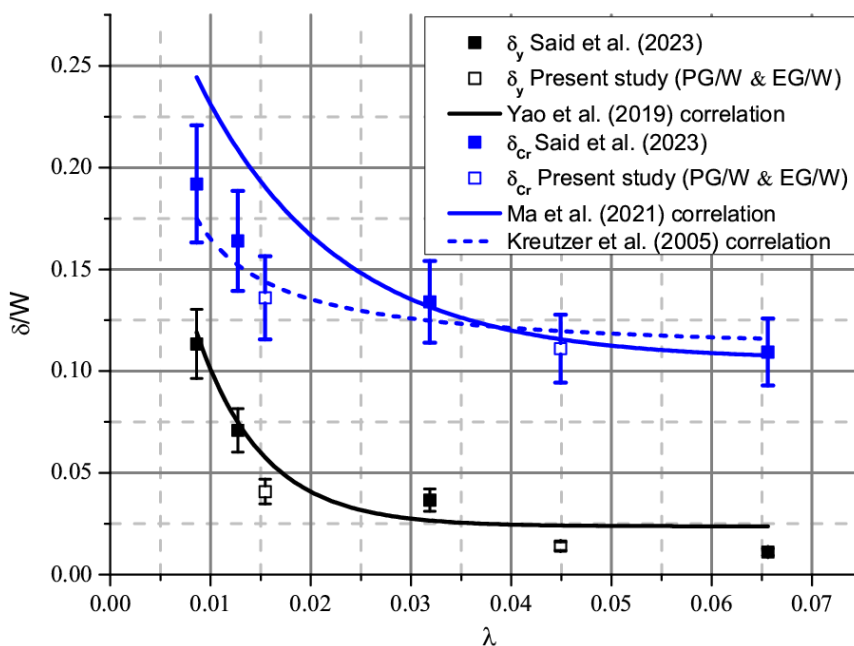


Fig. 7. δ_y and δ_{cr} versus experimental correlations and numerical results of Said et al. [40].



3.3. Heat transfer

To evaluate the heat transfer rate, the Nu number represented in Eq. (9) is used [46]. As mentioned, earlier, uniform heat flux is applied to the top and bottom walls of the microchannel (See Fig. 8):

$$Nu = \frac{q_w D_h}{k_c (T_w - T_{bulk,f})} \tag{9}$$

where q_w is the wall heat flux, D_h is the hydraulic diameter, k_c is the thermal conductivity of the continuous phase (EG or PG), T_w is the inner wall temperature and $T_{bulk,f}$ is the bulk fluid temperature. It is worth noting that the bulk fluid temperature $T_{bulk,f}$ is instantaneously calculated as a mass-weighted average value at different locations (planes) along the axial direction. On the other hand, the wall temperature T_w in the heated section is also calculated instantaneously as an area-weighted average value.

A constant flow rate of $Q = 0.4$ mL/min is chosen in this study for both fluid combinations (EG/W and PG/W), which corresponds to a mixture velocity U_{TP} of 0.037 m/s (See Table 2). Choosing this mixture velocity gives us the ability to produce the same droplet/slug length in the case of a T-junction for a flow rate ratio $Q_d/Q_c = 1$. The water patches, marked at the microchannel's entrance, gradually developed in the entrance region before entering the heated section. The droplet development process for the ethylene glycol (EG)/water (W) case is shown in Fig. 9.

Once the droplets reach their final shape, it can be seen that they are separated from the microchannel walls by a thin liquid film. It is worth mentioning that the droplets are more confined along the Z axis than the Y axis. It can also be seen that the front curvature of the droplet is steeper than the back one. This is mainly due to the force exerted by fluid motion inside the droplets at the front interface [28].

Three main parts were discussed in this work with a particular attention focused to the heated microchannel section. The water droplets are considered hydrodynamically developed at the heated section entrance.

In the first part of this work, the viscosity of the working fluids is assumed to be constant. Furthermore, an effect analysis of changing the heat flux effect on the heat transfer rate will be performed at the end of the section. In the second part, the viscosity of the working fluids is considered temperature dependent while the remaining properties (*density, thermal conductivity, ...*) are assumed to be constant. This is accomplished by implementing a user-defined function in the ANSYS Fluent software. The temperature-dependent viscosity effects on heat transfer rate, liquid film, droplet length, and droplet shape will be discussed. Finally, a third section will discuss the conjugate heat transfer effect on heat transfer rate.

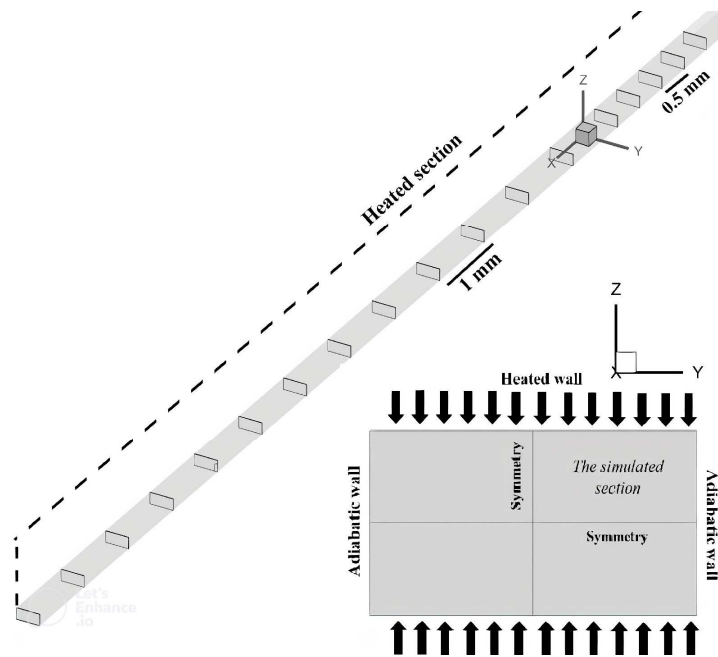


Fig. 8. Selected positions for recording bulk fluid temperatures as well as wall temperature.

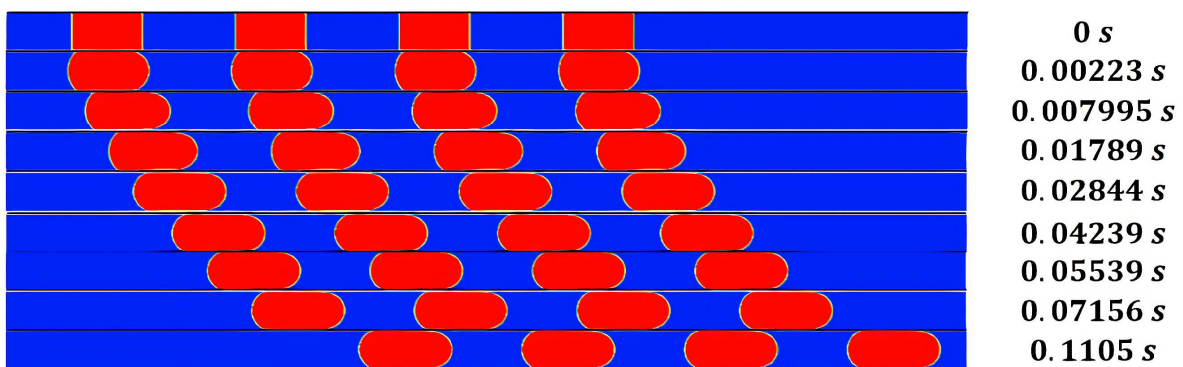


Fig. 9. Development and preparation stage of the water patches.



3.3.1. Constant working fluid properties

Tables 1 and 2 present the working fluids' thermophysical properties and input parameters employed in this research. Using ethylene glycol (EG) or propylene glycol (PG) as a carrier fluid, water droplets were dispersed periodically to create a liquid-liquid Taylor flow. As a result, recirculation zones appear in both the carrier fluid (continuous phase) and inside the droplets, which is the main reason for heat transfer enhancement in the microchannels. Among the studies available in the literature [25, 21], liquid-liquid Taylor flow has shown a remarkable increase in heat transfer rate over single-phase flow and gas-liquid Taylor flow.

Figure 10 shows the mid-droplet temperature contour for the EG/W combination. It can be seen that the bulk fluid temperature increases as it approaches the microchannel outlet. Taking a single cross-section, we can see that the temperature at the microchannel corners is higher than at the microchannel center (inside the droplets). This could be explained by the fact that the flow rate at the corners of the microchannel is lower than the global flow rate. This allows the carrier fluid (ethylene glycol) to absorb a higher amount of heat. Since ethylene glycol has a lower specific heat capacity than water, the latter becomes thermally saturated far faster than water.

Figure 11 shows the instantaneous temperature of the wall, the bulk fluid, as well as the Nu number in an axial section ($L_{th}/D_h=17.5$ from the entrance of the heated section) during water droplets passage. It can be seen from initial viewing that both the wall temperature T_{wall} and the bulk fluid temperature $T_{bulk,f}$ was continuously rising before the first water droplet passed through. However, once water droplets pass through the selected cross-section, oscillating behaviour can be seen at both T_{wall} and $T_{bulk,f}$. This is because the dispersion of water droplets within a carrier fluid induces mixing both in the continuous phase and within the water droplets. This promotes a decrease in both T_{wall} and $T_{bulk,f}$.

For better understanding, we have plotted the instantaneous variation of wall temperature, bulk fluid, and Nu number for a single unit cell (a water droplet and a slug) as depicted in Fig. 12.

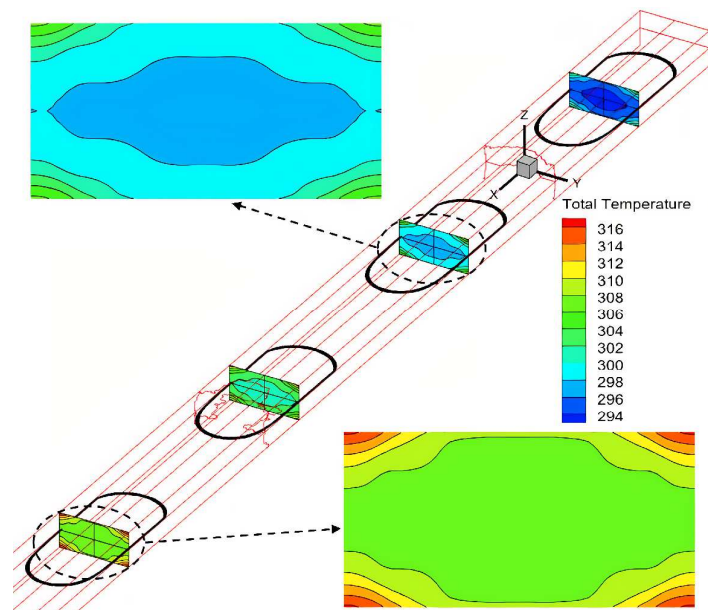


Fig. 10. Temperature contours at the center of the droplets at different sections.

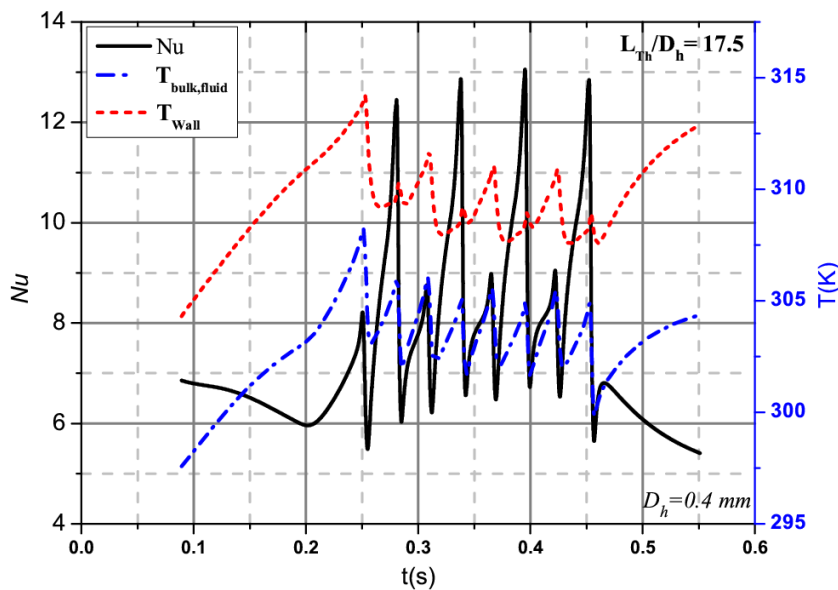


Fig. 11. Instantaneous variation of the Nu number, T_{wall} and $T_{bulk,f}$ in a fixed axial position.



As the water droplet passes through the selected axial section, a temperature decrease is observed both at the wall and within the flow (bulk fluid). This temperature reduction may be explained by the fact that hot fluid near the heated wall within the water droplet is transported to the centerline of the microchannel, while fresh fluid is brought back to the near-wall region [47]. As a result, the bulk fluid's temperature once again begins to increase as well as that of the heated wall. However, the increase in wall temperature was relatively insignificant compared to the increase in bulk fluid temperature, resulting in the smallest temperature difference ΔT between the heated wall and the bulk fluid temperature.

Using Eq. (9), the small temperature difference leads to the occurrence of Nu number peak as can be seen in Fig. 12. As the plug region passes through the selected axial section, a further temperature drop of the bulk fluid is observed, while a small temperature drop is observed at the heated wall. A possible reason for this is the fact that the presence of the EG/W interface causes a flow disturbance that leads to the appearance of two counter-rotating vortices enhancing mixing inside the flow. Similar observations were also reported in the literature, experimentally by Oliver and Young and analytically by Muzychka et al. [48] who noted that such a flow pattern (*dispersed bubbles within a continuous phase* "Taylor flow") induces both a change in velocity profile within the slugs as well as a presence of recirculation zones.

Figure 13 shows the instantaneous Nu for the EG/W combination at different dimensionless axial sections (L_{th}/D_h) along the microchannel. It is clear from Fig. 13. that the instantaneous Nu is independent of the axial section. For each axial position, we can identify 8 peaks in the instantaneous Nu which indicates the existence of recirculation zones both in the continuous phase and inside the droplets. The small peaks represent the ethylene glycol slug, while the large peaks correspond to water droplets. Thus, it is clear that heat transfer is much more efficient through the water droplets due to the superior thermal properties of water compared to ethylene glycol. Similar Nu number behaviour has previously been reported in Vivekanand et al.'s [29] and Chandrasekhar et al.'s [32] numerical studies of liquid-liquid two-phase systems.

The instantaneous Nu number for the two considered combination of the fluids, namely EG/W combination and PG/W combination is presented at four axial positions on Fig. 14.

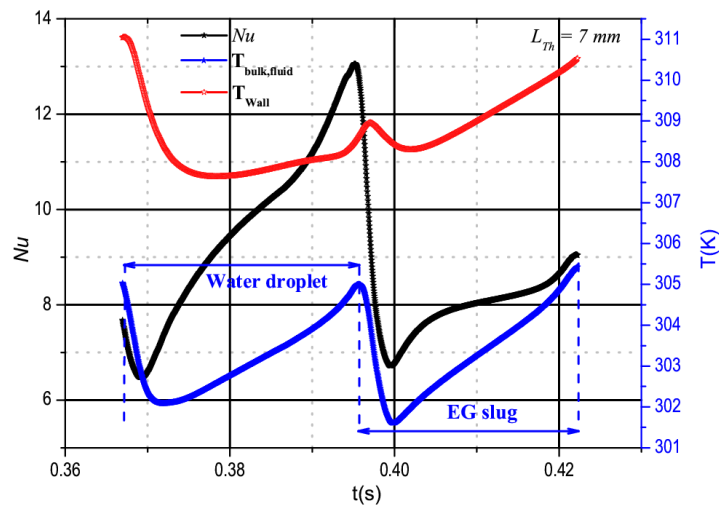


Fig. 12. Instantaneous variation of the Nu number, T_{wall} and $T_{bulk,f}$ in a unit cell (water droplet and slug).

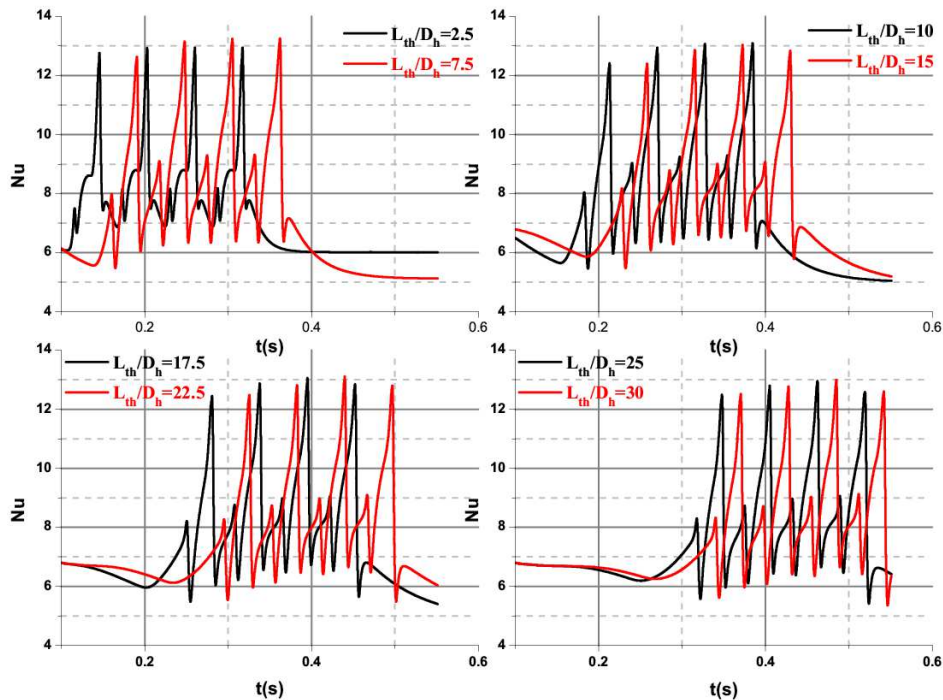


Fig. 13. Instantaneous Nu number for different axial positions along the microchannel.



It should be noted here that the input parameters ($Q = 0.4$ mL/min) are the same for both combinations (see Table 2).

The dimensionless distance, of the considered sections, from the heated section entrance are: $L_{th}/D_h = 2.5, 10, 17.5,$ and 25 . At the first axial section (2.5), we can see that the EG/W combination passes faster than the PG/W combination. The time shift occurring between the two combinations can be explained by the fact that the water droplets in the EG/W case move a smaller distance, before reaching the first axial section, than in the PG/W case. However, as the water droplet velocity (U_D) in the PG/W case is higher than in the EG/W case, the time shift gradually decreases as we move downstream of the heated section (10...).

Water droplet length is one of the parameters affecting heat transfer rate. According to Abdollahi et al. [19], the heat transfer rate increases with increasing water fraction volume for a constant unit cell length. EG/W and PG/W combination had dimensionless unit cell lengths of $L_{UC}/D_h = 6.18$ and $L_{UC}/D_h = 5.33$, respectively. However, water droplets occupied 59% and 58% of the unit cell length for the EG/W and PG/W combinations, respectively. Hence, the effect of water droplet length on heat transfer rate is almost the same in both cases. Furthermore, the slug length for EG/W and PG/W was $L_s/D_h = 2.53$ and 2.33 , respectively. This corresponds respectively to 41% and 42% of the unit cell length. Using a constant unit cell length and water as the disperse phase, Abdollahi et al. [19] stated that the smaller the slug length, the higher the recirculation zones will be with a significant radial velocity. Moreover, they indicated that an optimum slug length of $L_s/D_h = 5$ provides an optimal heat transfer rate with a low friction coefficient.

For the present study, the slug lengths are almost the same for both combinations. This results in a reasonable heat transfer rate, reflected by the small peaks observed in the instantaneous Nu number. However, the Nu peaks for EG/W seem higher than those for PG/W. One possible explanation is that EG's heat capacity is superior PG's.

Another parameter capable of affecting the heat transfer rate is the liquid film thickness. As measured along the z -axis, the liquid film between the water droplet and the heated wall is 1.4% ($4.2 \mu\text{m}$) and 2.3% ($7 \mu\text{m}$) of the microchannel depth h in the EG/W and PG/W cases, respectively. Due to the low flow rate through the liquid film region and the no-slip conditions at the wall as well as at the interface between the two phases, heat transfer within the liquid film is often done by conduction rather than by convection [19]. However, the low thermal conductivity of liquids (0.26 and 0.19 W/m-K for EG and PG, respectively), causes the liquid film of the continuous phase to act as an insulator preventing the water droplet from properly transporting heat from the heated wall to the fluid [11]. Furthermore, for the PG/W case, the water droplet is less confined along the y -axis, resulting in a thicker liquid film both at the corners ($82 \mu\text{m}$) and along the y -axis (4.1% of the channel width W). Indeed, this increase in the liquid film thickness will, on one side, induce an increase in the flow rate through the film region and, on the other side, decrease the intensity and volume of the recirculation zone as well as the radial mixing. In previous numerical investigations in gas-liquid systems, Abadie et al. [49] have shown that the transport process (*heat or mass*) could be hindered by a decrease in the recirculation volume caused by an increase in the Ca number (*increase in the liquid film*).

A similar observation was made by Zhang et al. [10]. Talimi et al. [50], in their numerical analysis of the effect of liquid film thickness on heat transfer for a Taylor gas-liquid flow, revealed that the flow bypasses through the liquid film area is the main reason for the reduction in heat transfer rate as it contributes to the shrinking of the recirculation zone in the continuous phase. However, the heat transfer rate in both cases is still higher than the single-phase flow of ethylene and propylene glycol. This shows the importance of the recirculation zones within the two phases.

Figure 15 gives the local Nu number variation as well as the temperature difference between the wall and the bulk fluid for both EG/W and PG/W cases. The local Nu was calculated by averaging the wall and bulk fluid temperatures for each axial section during the passage of the water droplets (see Fig. 8). Figure 15 shows that the temperature difference ($T_{wall} - T_{bulk,i}$) in the EG/W case is smaller than in the PG/W case. This results in a better heat transfer rate for the EG/W combination. The temperature difference ΔT , for EG/W, is about 5.5 K, whereas, for PG/W, the temperature difference is 2.5 K higher than EG/W at a temperature difference of about 8 K. As a result, the local Nu number is larger in the EG/W case than in the PG/W case, with an average value of around 8.5 ($Nu_{EGW} = 8.5$). As compared to single-phase flow, liquid-liquid Taylor flow for both EG/W and PG/W cases exhibits a much higher heat transfer rate. The average local Nu number increases by more than 440% in the EG/W case relative to the single-phase flow of ethylene glycol ($Nu_{SP,EG} = 1.94$) with same inlet flow rate. Likewise, the PG/W case showed an improvement of over 370% ($Nu_{PGW} = 7.6$) compared to a single-phase propylene glycol flow ($Nu_{SP,PG} = 2.03$) with the same inlet flow rate.

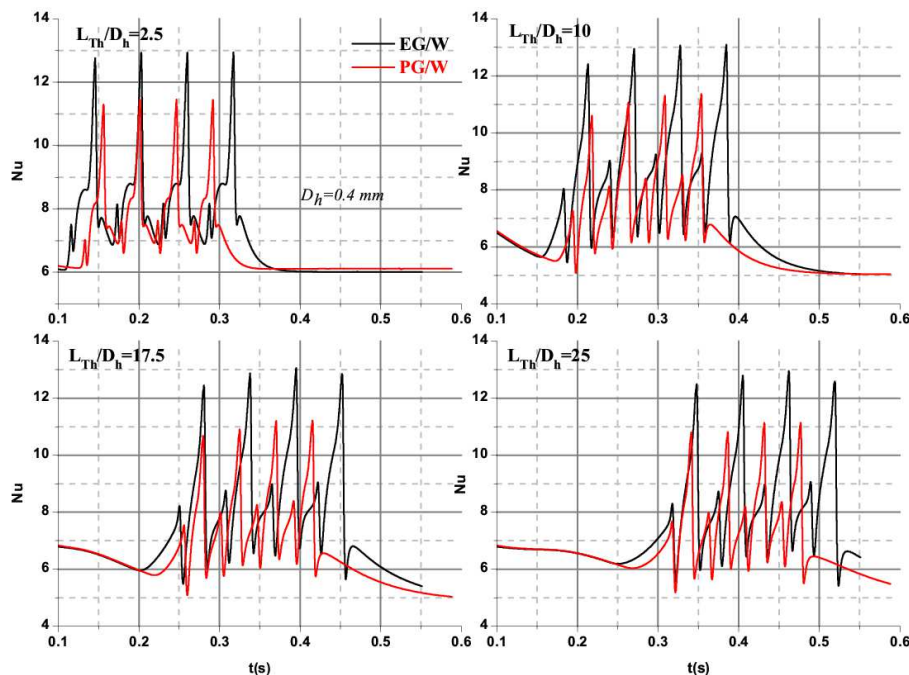


Fig. 14. The instantaneous Nu number for both PG/W and EG/W cases at different axial positions.



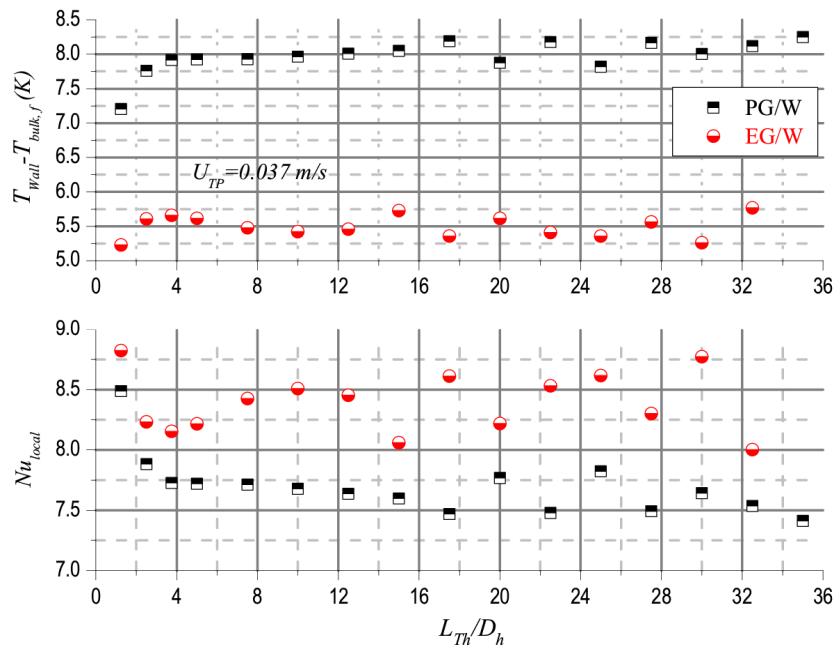


Fig. 15. Local Nu number and temperature difference ($T_{wall}-T_{bulk,f}$) for EG/W and PG/W.

Several studies in the literature [11, 19, 21, 22] confirm the improvement provided by Taylor liquid-liquid flow regarding heat evacuation in microchannel heat sinks. However, the enhancement rate varies between studies and depends on several factors, such as channel geometry, working fluids, thermal boundary condition, and inlet parameters (flow rate of both phases).

In the experimental and numerical heat transfer study of Taylor flow in a square microchannel [19], the authors reported a heat transfer improvement of up to 700% over single-phase flow. Asthana et al. [21] achieved, in their experiment, a heat transfer rate four times superior to that of a single-phase flow in a square serpentine microchannel. In a 3D numerical study on a rectangular microchannel with different aspect ratios, Chandrasekhar et al. [32], reported an improvement in heat transfer of 222% relative to a single-phase flow in situations where the microchannel's opposite walls were used as a thermal boundary condition.

3.3.2. Temperature dependence of working fluid viscosity

Understanding the dependence of liquid viscosity on temperature is an important factor in many engineering applications. In this section, the working fluids, namely ethylene, propylene glycol and water are temperature dependent using a UDF implemented in ANSYS Fluent. The correlations employed are available in the literature [51, 52] and are thus listed in Table 6. All other parameters (inlet flow rate, length of patches...) are the same as those used in the first section as well as in the validation. As discussed earlier, the water droplet length L_D , the slug length L_s of the continuous phase (distance between the two droplets), and the liquid film thickness (δ_{cr} , δ_y , δ_z), are the main parameters that affect the heat transfer rate. For this reason, we were interested in closely examining the effect of temperature-dependent viscosity variation of the working fluids on the behavior of liquid-liquid Taylor flow (L_D , L_s ...) and on the heat transfer rate represented by the Nu number. The same combinations were chosen as in the first section, i.e., EG/W and PG/W.

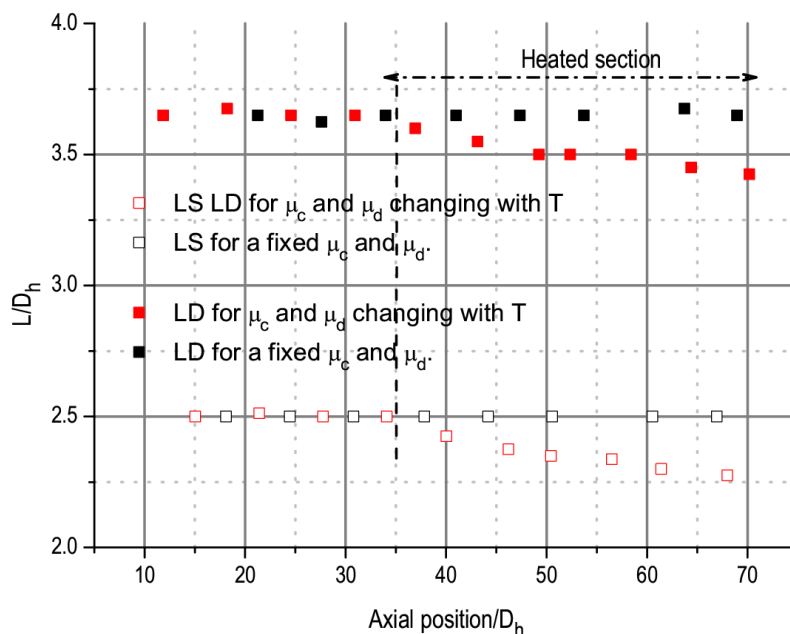


Fig. 16. L_D et L_s variation along the microchannel for EG/W case.



Table 6. Typical working fluid viscosity correlations depending on T.

Working fluid	Correlation	Reference
Water	$\mu_w = (1.435 \cdot 10^{-5})e^{\frac{1227}{T}}$	[48]
Ethylene glycol	$\mu_{EG} = (1.6 \cdot 10^{-7})e^{\frac{3340}{T}}$	[48]
Propylene glycol	$\mu_{PG} = 0.015238e^{\left(\frac{1057.801}{T-T_0}\right)}$ with $T_0 = 165K$	[49]

Figure 16 shows the variation of L_D and L_s along the microchannel as the viscosity of both liquids (EG and W) varies with temperature.

Before reaching the heated section, the water droplet length and slug length remain unchanged and are identical to L_D and L_s in the case of constant fluid properties. However, as the droplets cross the heated section, L_D and L_s decrease progressively at almost the same level and degree of decay. A decrease of 6.2% was seen in the water droplet length close to the microchannel outlet, whereas a decrease of 9% was noted in the slugs. This decrease observed in L_D and L_s will somehow impact the heat transfer performance. To visualize this, the instantaneous Nu number for the EG/W combination with and without temperature-dependent viscosity was plotted (see Fig. 17).

As can be observed, at the entrance to the heated section, the instantaneous Nu number trend is the same in both cases. This is due to slight variations in the liquid film thickness as well as L_D and L_s . However, as one moves toward the outlet of the microchannel, the Nu peak in the T-dependent viscosity case starts to gradually increase, with the Nu curve shifting to the right. The increase in the Nu peak may be explained by the decrease in L_D , L_s , and the liquid film while moving toward the microchannel outlet. Furthermore, the shift in the Nu curve results from the increase in the droplets' velocity caused by the decrease in the viscosity of both phases.

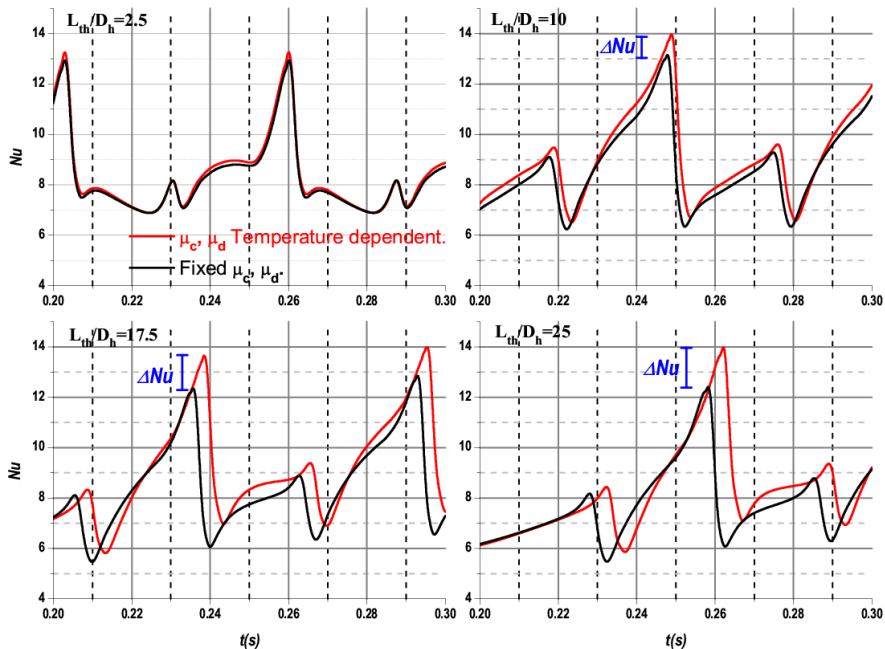


Fig. 17. The instantaneous Nu number for both EG/W cases at different axial positions.

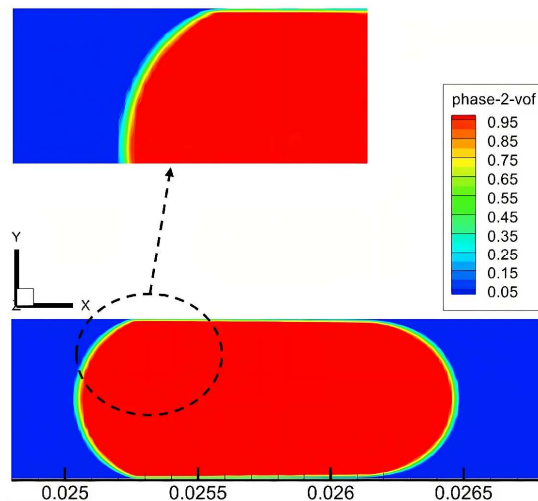


Fig. 18. The non-appearance of the liquid film near the microchannel outlet.



It is worth mentioning that because of viscosity decrease with T , the liquid film thickness becomes extremely small near the microchannel outlet (see Fig. 18), especially at the water droplets rear. This prevents us from capturing it even with mesh refinement close to the walls.

Therefore, we were unable to analyze the effect of viscosity dependence, especially the effect of the liquid film thickness variation on heat transfer rate. To achieve this, we performed the same investigation with propylene glycol as the continuous phase and water as the dispersed phase (PG/W), with viscosities that are T dependent.

Figure 19 shows the variation of dimensionless L_D and L_S along the microchannel. As mentioned earlier, the droplet and slug lengths remain unchanged before entering the heated section. However, once the droplets arrived in the heated section, a significant reduction in droplet and slug lengths was observed.

Compared to the EG/W case, the degree of decrease here (PG/W) was larger with a percentage, near the microchannel outlet, of 13.31% and 22.7% for L_D and L_S respectively. This significant diminution in the slug length compared to the droplet length is due to the temperature effect on the working fluids' viscosity. Particularly its effect on the continuous phase viscosity μ_c (propylene glycol) which was found to have more impact on L_D and L_S than that of the dispersed phase μ_d (water).

To closely examine the behavior of the water droplet in the heated section, we presented in Fig. 20 the volume fraction contours showing the droplet interface deformation at different axial positions along the heated section.

At the entry of the heated section, the water droplet maintains its shape due to small variations in μ_c and μ_d . As we move through the heated section, a variation in the liquid film thickness ($\delta_y, \delta_z, \delta_{Cr}$) as well as in the droplet length L_D is observed. This leads to droplet shrinking on the x -axis along with confinement on the y -axis. The reduction in liquid film thickness is attributed to the substantial decrease in the continuous phase viscosity compared to that of the dispersed phase. Consequently, a progressive reduction in the viscous shear exerted by the continuous phase on the droplet interface was observed, resulting in a diminution of the liquid film thickness.

Figure 21 shows the effect of the temperature dependence of μ_c and μ_d on the liquid film thickness along the y and z axes. It is clear from Fig. 21 that the liquid film thickness in both directions (δ_y and δ_z) decreases progressively as the plug moves through the heated section. However, the decrease in film thickness in the y -direction (δ_y) was more pronounced than in the z -direction (δ_z), leading to the confinement of the droplet along both axes.

Based on the previous discussion, the variation of the liquid film thickness as well as L_D and L_S will certainly have an impact on the heat transfer rate for Taylor liquid-liquid flow.

For the PG/W case, where μ_c and μ_d are temperature-dependent, Fig. 22 illustrates the instantaneous Nu number at four axial sections along the heated section. The behavior of the instantaneous Nu between the two cases (μ_d, μ_c with and without temperature dependency) remains the same regardless of the chosen axial position. However, the magnitude of the instantaneous Nu for T -dependent viscosities is higher, with a ΔNu that increases moving toward the microchannel outlet. This increase in instantaneous Nu is the result of both variations in droplet and slug length (L_D, L_S), but more specifically the variation observed in the liquid film thickness. Variation in the liquid film thickness in the y -, z -direction (δ_y, δ_z) as well as in the corners (δ_{Cr}) leads to droplet confinement in both directions.

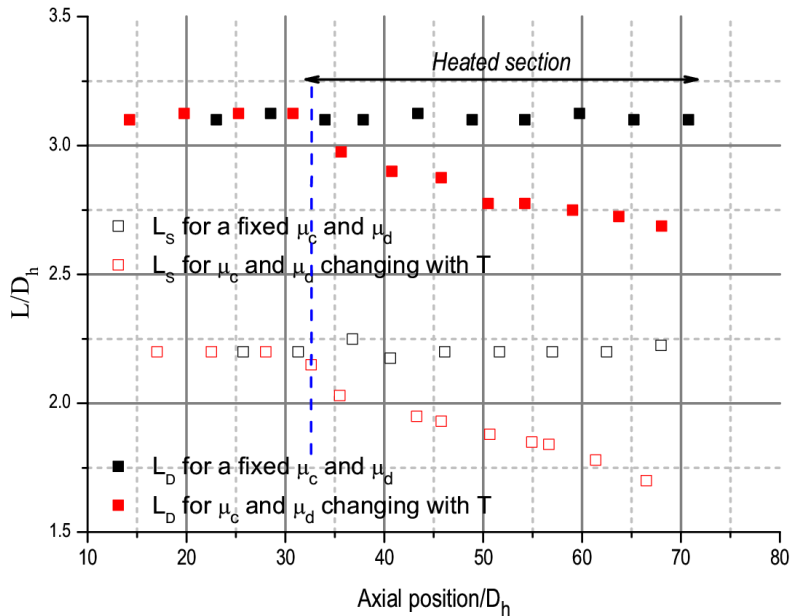


Fig. 19. L_D et L_S variation along the microchannel for PG/W case.

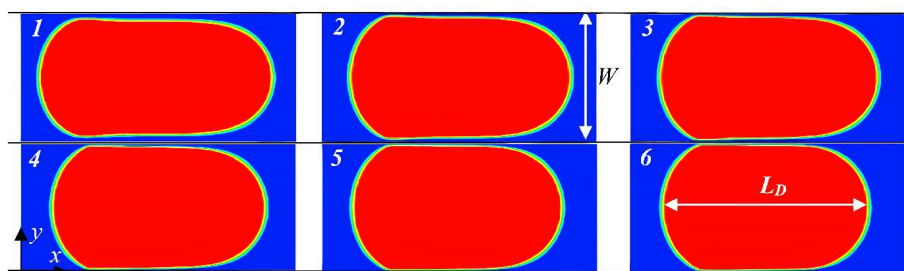


Fig. 20. Deformation of PG/W interface along the microchannel.



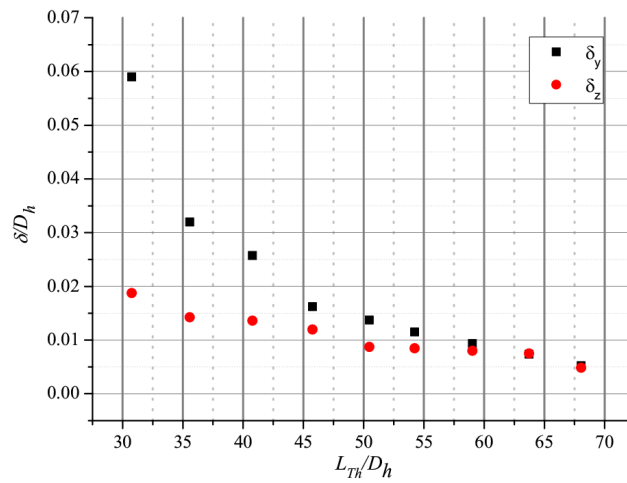


Fig. 21. Variation of δ_y and δ_z along the heated section for the PG/W case.

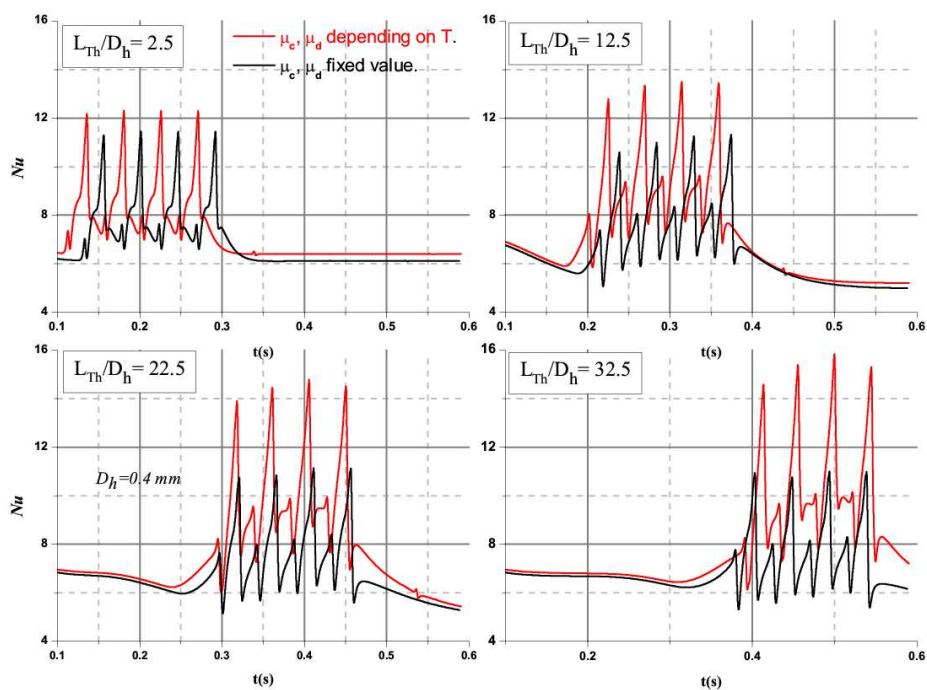


Fig. 22. The instantaneous Nu number for both PG/W cases at different axial positions.

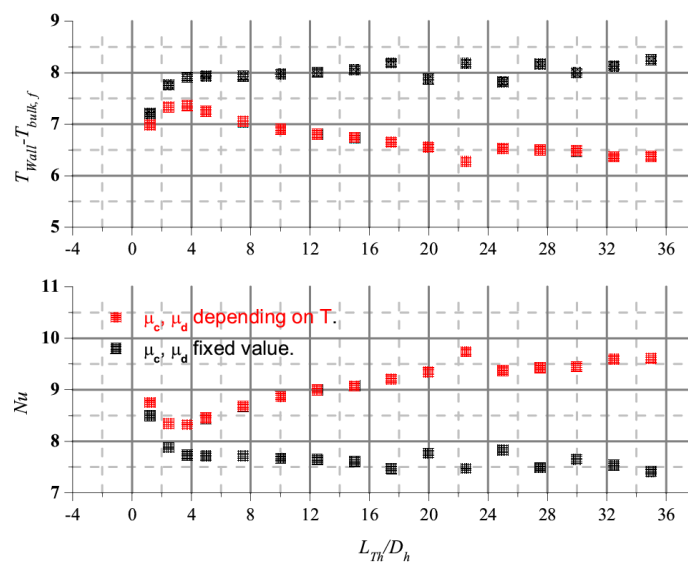


Fig. 23. Nu and $(T_{wall} - T_{bulk,t})$ for PG/W case with μ_c and μ_d temperature-dependent.



As a result, less fluid is bypassing through the liquid film region, which increases the recirculation zone volume (*decreasing the recirculation time*) where most of the continuous phase fluid is circulating within the slug (*increasing the radial mixing*). Similar observations have been reported earlier in literature for gas-liquid Taylor flow [50, 49, 10].

A comparison of local *Nu* number and $(T_{wall}-T_{bulk,i})$ for PG/W with and without viscosity temperature dependence is presented in Fig. 23. The local *Nu* was calculated by averaging the wall and bulk fluid temperatures for each axial section during the passage of the water droplets. At the entrance to the heated section, the temperature difference $(T_{wall}-T_{bulk,i})$ is comparable to that of PG/W where the fluid properties are constant. However, as we gradually proceed through the heated section, the gap in $(T_{wall}-T_{bulk,i})$ starts to increase as a consequence of the aforementioned variations in the liquid film thickness as well as in L_D and L_s . This reduction in the temperature difference between the wall and the bulk fluid induces effective heat transfer, indicated by the local *Nu* number. This latter was shown to gradually increase as we move toward the microchannel outlet, with an average value of around 9.1. An increase of about 20.4% in the average local *Nu* number was noticed when fluid properties, particularly viscosity, are temperature dependent, compared to constant fluid properties.

3.3.3. Conjugate heat transfer

In the previous sections, we assumed that the microchannel walls had no thickness. However, experimentally, microchannel walls are often made of a thermally conductive material whose layer thickness could be even thicker than the height or width of the microchannel. In this section, the effect of adding a wall thickness of 50 μm “which is 1/6 the height of the microchannel”, assumed to be made of aluminum, on heat transfer performance was investigated (see Fig. 24). Propylene glycol and water combination (PG/W) is used here under the same parameters as in the previous sections.

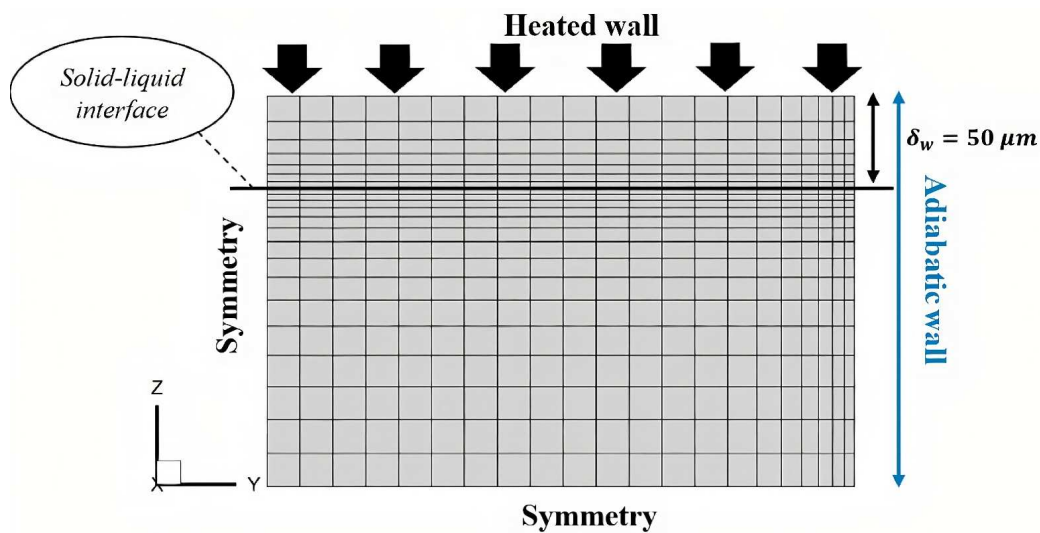


Fig. 24. schematic diagram of the microchannel cross-section with the corresponding parameters.

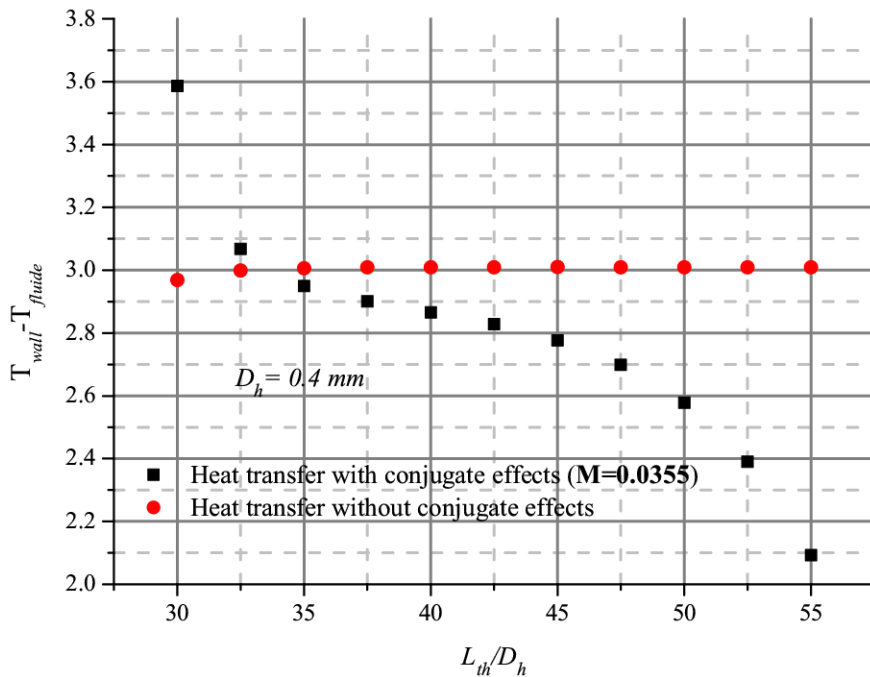


Fig. 25. $\Delta T = T_{wall} - T_{fluid}$ with and without conjugate heat transfer effects.



For micro and mini-scale geometries, conjugate heat transfer effects could have a significant impact. To quantify the axial conduction effect, Maranzana et al. [53] developed a criterion based on single-phase flow in a rectangular mini channel. It was determined that axial conduction in the mini/microchannel wall becomes significant with a high axial conduction number $M \geq 0.01$:

$$M = \frac{1}{(\text{RePr})} \left(\frac{D_h}{L_{th}} \right) \cdot \left(\frac{\delta_w}{h} \right) \cdot \left(\frac{k_w}{k_f} \right) \quad (10)$$

where Re , Pr , L_{th} , D_h , δ_w , h , k_w , k_f are respectively the Reynolds and Prandtl number, the length of the heated section, the hydraulic diameter, the thickness of the solid wall (50 μm), the height of the microchannel (fluid domain), the thermal conductivity of the solid (aluminium), and the thermal conductivity of the fluid (Propylene glycol).

We calculated the axial conduction number in our study, and the value of M was higher than 0.01 ($M = 0.0355$), which proves the presence of axial conduction effects at the solid wall. To validate this, a numerical simulation of a single-phase flow of propylene glycol with and without conjugate transfer effects was conducted (see Fig. 25).

Figure 25 shows the temperature difference between the wall and the fluid ($T_{\text{wall}} - T_{\text{fluid}}$) with and without conjugate heat transfer effects. The wall temperature T_{wall} at each axial section was calculated by averaging the wall temperature along a line along the heated wall (or at the solid/liquid interface in case conjugate transfer effects are introduced). A similar procedure was used to calculate the fluid temperature near the heated wall. Without assuming conjugate heat transfer effects, T_{wall} and T_{fluid} increase linearly in the thermally developed zone. That's why the temperature difference between the wall and the fluid ($T_{\text{wall}} - T_{\text{fluid}}$) remains constant throughout the microchannel (see Fig. 25).

However, when the conjugate effects are considered with a high axial conduction number ($M = 0.0355$), a remarkable change occurs in the wall and fluid temperature behaviour. Wall and fluid temperature behaviour within the thermal development zone shows non-linear behaviour. This results in a temperature difference ($T_{\text{wall}} - T_{\text{fluid}}$) that changes along the heated section (Fig. 24). The main reason is local heat flux variation at the liquid-solid interface (Fig. 26) caused by axial conduction effects on the solid substrate [53]. The constant heat flux condition applied to the outer surface of the microchannel wall is believed to be deformed due to the high value of M .

Figure 26 shows the heat flux ratio between that at the liquid-solid interface and that applied to the outer wall along the heated section. As can be seen, a non-uniformity of heat flux, particularly near the inlet and outlet of the heated section, is apparent at the liquid-solid interface. Mehta et al. [54], investigated numerically the effect of axial conduction in a square microchannel using single-phase flow. It was found that axial conduction (expressed as an axial conduction number $M \geq 0.01$) could strongly influence the heat flux ratio at the liquid-solid interface, the wall temperature, and the fluid temperature.

In the liquid-liquid Taylor flow case, and for the PG/W combination, the heat transfer performance will certainly be affected by the effects of axial conduction within the microchannel substrate. As discussed earlier, heat transfer from the inner wall to the liquid film is mainly done by conduction due to the low flow rate through this region [19]. As a result, the film temperature is often the same as the microchannel inner wall temperature.

Figure 27 shows the instantaneous wall and bulk fluid temperatures for several dimensionless axial sections along the heated section. In each dimensionless axial section, and as previously mentioned, oscillations occur in the instantaneous bulk fluid and wall temperature caused by the passage of water droplets. However, the oscillation amplitude in the instantaneous wall temperature decreases progressively towards the microchannel outlet. This finding differs from what was previously observed in Section 1. One possible reason is the non-uniform heat flux at the liquid-solid interface, which can significantly affect the wall temperature.

The instantaneous Nu for different dimensionless axial sections along the heated section is shown in Fig. 28. The instantaneous Nu behaviour as water droplets pass through the various axial sections is the same as observed previously. However, the Nu number magnitude increases as one progresses through the heated section. This increase in heat transfer rate could be explained by the low ΔT between the wall and the bulk fluid downstream compared to upstream of the heated section. This difference in ΔT is mainly due to the variation in local heat flux at the liquid-solid interface (see Fig. 26).

It is necessary to do more research in the conjugate heat transfer and axial conduction domain, as these factors significantly influence the heat transfer performance of two-phase Taylor flows in mini and microchannels.

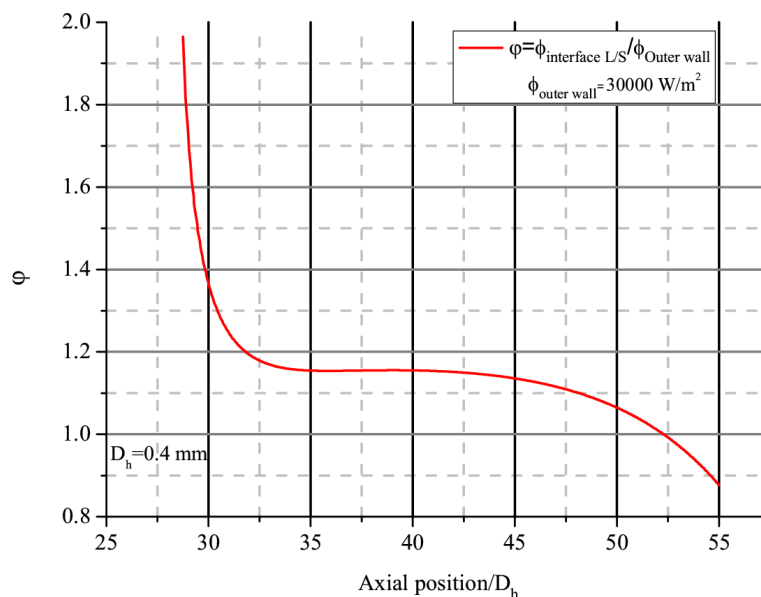


Fig. 26. The heat flux ratio between the liquid-solid interface and the outer wall across the heated section.



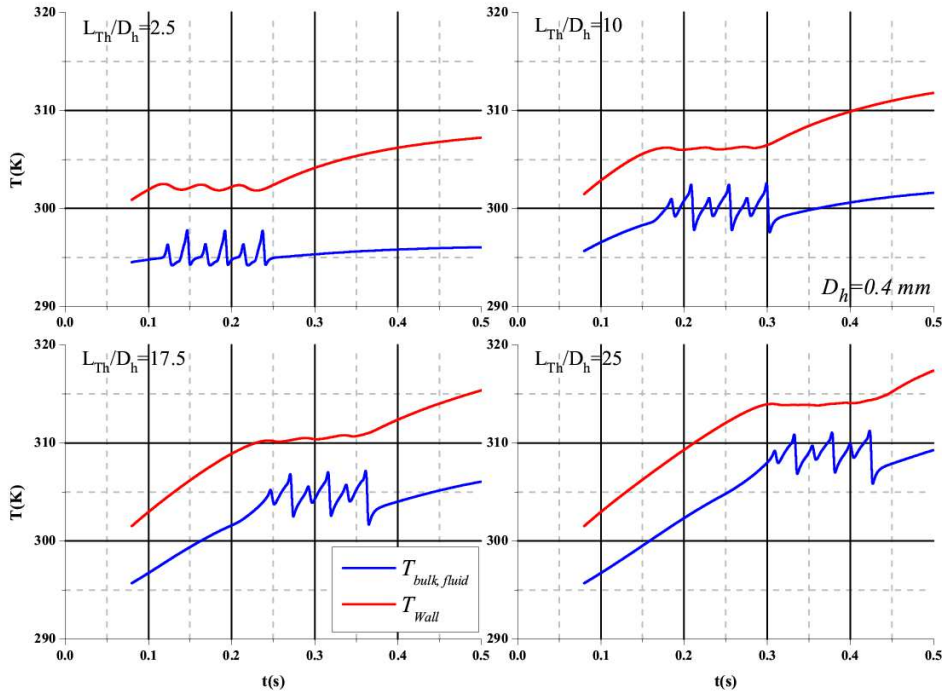


Fig. 27. the instantaneous T_{wall} and $T_{bulk,f}$ for several positions along the heated section.

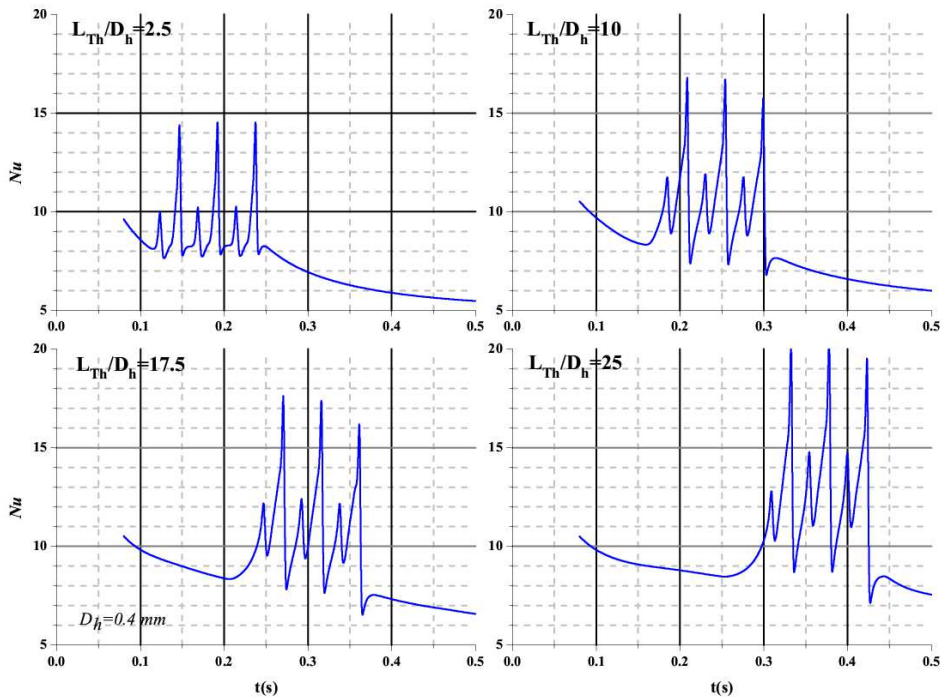


Fig. 28. Instantaneous Nu for several position along the heated section.

4. Conclusion

A 3D numerical study investigating the heat transfer performance of liquid-liquid Taylor flow in a rectangular microchannel was performed using the commercial software ANSYS Fluent. A Volume of Fluid (VOF) method was applied to capture and track the interface between the two phases. The mesh size was refined near the microchannel walls to enable capturing the liquid film between the dispersed phase and the walls with an acceptable computational time. To evaluate Taylor flow effect on heat transfer performance, two fluids combinations were used in which water droplets are dispersed in a carrier phase of either ethylene or propylene glycol, with initially constant thermo-physical properties. Then, we considered the viscosity of the working fluids to be temperature dependent to examine its effect on droplet behaviour and heat transfer rate. The conjugate transfer and axial conduction effect were also studied with a 50 μ m aluminium wall thickness. The results showed that the liquid film in the corners (δ_{cr}) or along the y - or z -axis (δ_z, δ_y) significantly affects the recirculation volume and radial mixing, thus directly influencing the heat transfer rate. It has been shown that instantaneous viscosity changes in the continuous and dispersed phase result in a change in droplet and slug topology (a decrease in L_D and L_s , a change in droplet shape) along with a reduction in liquid film thickness ($\delta_y, \delta_z, \delta_{cr}$), thus affecting the heat transfer rate. The axial conduction phenomenon in the solid substrate was also studied. It has been



noticed that the local heat flux at the liquid-solid interface could be affected by the axial conduction, consequently changing the heat transfer performance. Finally, this study could help to fully understand the effects of instantaneous changes in working fluid viscosity on heat transfer performance. It may also assist in understanding the conjugate transfer when designing an experimental facility with a micro or mini-scale geometry.

Authors Contributions

M. SAID developed the numerical model, conducted the simulations, wrote the manuscript, and prepared all the figures under the other co-author's guidance. All authors discussed the results, reviewed, and approved the final version of the manuscript.

Acknowledgments

Not applicable.

Conflict of Interest

The authors declare that they don't have any conflict of interest.

Funding

No funding was received for conducting this study.

Data Availability Statements

The datasets generated and/or analyzed during the current study are available from the corresponding author on reasonable request.

Nomenclature

W	Microchannel width [m]	δ	Film thickness
L	Length [m]	c	Continuous phase
h	Microchannel height [m]	d	Dispersed phase
D_h	Hydraulic diameter [m]	UC	Unit cell
A	Cross-section area [m ²]	TP	Two-phase
U	Velocity [m/s]	D	Droplet/plug
T	Temperature [K]	Cr	Corner
q	Heat flux [kW/m ²]	PCB	Printed Circuit Board
Q	Flow rate [m ³ /s]		
\dot{Q}	Flow rate ratio		
Ca_{TP}	Capillary number of two-phase flow, $Ca_{TP} = \mu_c U_{TP} / \sigma$		
Ca_c	Capillary number of the continuous phase, $Ca_c = \mu_c U_c / \sigma$		
Ca_D	Capillary number based on plug velocity, $Ca_D = \mu_c U_D / \sigma$		
Nu	Nusselt Number		
M	Axial conduction number		
λ	Viscosity ratio, $\lambda = \mu_d / \mu_c$		

References

- [1] Agostini, B., Fabbri, M., Park, J.E., Wojtan, L., Thome, J.R., Michel, B., State of the art of high heat flux cooling technologies, *Heat Transfer Engineering*, 28(4), 2007, 258–281, 2007, doi: 10.1080/01457630601117799.
- [2] Japar, W.M.A.A., Sidik, N.A.C., Saidur, R., Asako, Y., Nurul Akmal Yusof, S., A review of passive methods in microchannel heat sink application through advanced geometric structure and nanofluids: Current advancements and challenges, *Nanotechnology Reviews*, 9(1), 2020, 1192–1216, doi: 10.1515/ntrev-2020-0094.
- [3] Go, J.S., Design of a microfin array heat sink using flow-induced vibration to enhance the heat transfer in the laminar flow regime, *Sensors & Actuators A*, 105(2), 2003, 201–210, doi: 10.1016/S0924-4247(03)00101-8.
- [4] Krishnaveni, T., Renganathan, T., Picardo, J.R., Pushpavanam, S., Numerical study of enhanced mixing in pressure-driven flows in microchannels using a spatially periodic electric field, *Physical Review E*, 96(3), 2017, 1–15, doi: 10.1103/PhysRevE.96.033117.
- [5] Hessami, M.A., Berryman, A., Bandopdhayay, P., Heat transfer enhancement in an electrically heated horizontal pipe due to flow pulsation, *ASME International Mechanical Engineering Congress and Exposition*, 37181, 2003, 49–56.
- [6] Alam, T., Lee, P.S., Yap, C.R., Effects of surface roughness on flow boiling in silicon microgap heat sinks, *International Journal of Heat and Mass Transfer*, 64, 2013, 28–41, doi: 10.1016/j.ijheatmasstransfer.2013.04.009.
- [7] Xie, G., Zhang, F., Sundén, B., Zhang, W., Constructural design and thermal analysis of microchannel heat sinks with multistage bifurcations in single-phase liquid flow, *Applied Thermal Engineering*, 62(2), 2014, 791–802, doi: 10.1016/j.applthermaleng.2013.10.042.
- [8] Sui, Y., Teo, C.J., Lee, P.S., Chew, Y.T., Shu, C., Fluid flow and heat transfer in wavy microchannels, *International Journal of Heat and Mass Transfer*, 53(13–14), 2010, 2760–2772, doi: 10.1016/j.ijheatmasstransfer.2010.02.022.
- [9] Zhou, Y.L., Chang, H., Numerical simulation of hydrodynamic and heat transfer characteristics of slug flow in serpentine microchannel with various curvature ratio, *Heat and Mass Transfer*, 55, 2019, 3343–3358, doi: 10.1007/s00231-019-02664-4.
- [10] Zhang, J., Fletcher, D.F., Li, W., Heat transfer and pressure drop characteristics of gas-liquid Taylor flow in mini ducts of square and rectangular cross-sections, *International Journal of Heat and Mass Transfer*, 103, 2016, 45–56, doi: 10.1016/j.ijheatmasstransfer.2016.07.007.
- [11] Eain, M.M.G., Egan, V., Punch, J., Local Nusselt number enhancements in liquid-liquid Taylor flows, *International Journal of Heat and Mass Transfer*, 80, 2015, 85–97, doi: 10.1016/j.ijheatmasstransfer.2014.09.009.
- [12] Xia, G.D., Liu, R., Wang, J., Du, M., The characteristics of convective heat transfer in microchannel heat sinks using Al₂O₃ and TiO₂ nanofluids, *International Communications in Heat and Mass Transfer*, 76, 2016, 256–264, doi: 10.1016/j.icheatmasstransfer.2016.05.034.
- [13] Kovalev, A.V., Yagodnitsyna, A.A., Bilsky, A.V., Flow hydrodynamics of immiscible liquids with low viscosity ratio in a rectangular microchannel



- with T-junction, *Chemical Engineering Journal*, 352, 2018, 120-132, doi: 10.1016/j.cej.2018.07.013.
- [14] Li, Q., Angeli, P., Experimental and numerical hydrodynamic studies of ionic liquid-aqueous plug flow in small channels, *Chemical Engineering Journal*, 328, 2017, 717-736, doi: 10.1016/j.cej.2017.07.037.
- [15] Eain, M.M.G., Egan, V., PUNCH, J., Film thickness measurements in liquid-liquid slug flow regimes, *International Journal of Heat and Fluid Flow*, 44, 2013, 515-523, doi: 10.1016/j.ijheatfluidflow.2013.08.009.
- [16] Ma, H., Zhao, Q., Yao, C., Zhao, Y., Chen, G., Effect of fluid viscosities on the liquid-liquid slug flow and pressure drop in a rectangular microreactor, *Chemical Engineering Science*, 241, 2021, 116697, doi: 10.1016/j.ces.2021.116697.
- [17] Abiev, R.S., Effect of contact-angle hysteresis on the pressure drop under slug flow conditions in minichannels and microchannels, *Theoretical Foundations of Chemical Engineering*, 49, 2015, 414-421, doi: 10.1134/S0040579515040223.
- [18] Abiev, R.S., Analysis of local pressure gradient inversion and form of bubbles in Taylor flow in microchannels, *Chemical Engineering Science*, 174, 2017, 403-412, doi: 10.1016/j.ces.2017.09.041.
- [19] Abdollahi, A., Norris, S.E., Sharma, R.N., Fluid flow and heat transfer of liquid-liquid Taylor flow in square microchannels, *Applied Thermal Engineering*, 172, 2020, 115123, doi: 10.1016/j.applthermaleng.2020.115123.
- [20] Adrugi, W., Muzychka, Y., Pope, K., Heat Transfer in Liquid-Liquid Taylor Flow in Miniscale Curved Tubing for Constant Wall Temperature, *Journal of Electronic Packaging*, 139(2), 2017, 020909, doi: 10.1115/1.4036405.
- [21] Asthana, A., Zinovik, I., Weinmueller, C., Poulikakos, D., Significant Nusselt number increase in microchannels with a segmented flow of two immiscible liquids: An experimental study, *International Journal of Heat and Mass Transfer*, 54(7-8), 2011, 1456-1464, doi: 10.1016/j.ijheatmasstransfer.2010.11.048.
- [22] Dai, Z., Guo, Z., Fletcher, D.F., Haynes, B.S., Taylor flow heat transfer in microchannels—Unification of liquid-liquid and gas-liquid results, *Chemical Engineering Science*, 138, 2015, 140-152, doi: 10.1016/j.ces.2015.08.012.
- [23] Abdollahi, A., *Fluid flow and heat transfer of liquid-liquid Taylor flow in microchannels*, Ph.D. Thesis, The University of Auckland, Auckland, New Zealand, 2019, <http://hdl.handle.net/2292/51345>.
- [24] Urbant, P., Leshansky, A., Halupovich, Y., On the forced convective heat transport in a droplet-laden flow in microchannels, *Microfluidics and Nanofluidics*, 4, 2008, 533-542, doi: 10.1007/s10404-007-0211-2.
- [25] Fischer, M., Juric, D., Poulikakos, D., Large convective heat transfer enhancement in microchannels with a train of coflowing immiscible or colloidal droplets, *Journal of Heat Transfer*, 132, 2010, doi: 10.1115/1.4002031.
- [26] Che, Z., Wong, T.N., Nguyen, N.T., Heat transfer enhancement by recirculating flow within liquid plugs in microchannels, *International Journal of Heat and Mass Transfer*, 55(7-8), 2012, 1947-1956, doi: 10.1016/j.ijheatmasstransfer.2011.11.050.
- [27] Che, Z., Wong, T.N., Nguyen, N.T., Yang, C., Three dimensional features of convective heat transfer in droplet-based microchannel heat sinks, *International Journal of Heat and Mass Transfer*, 86, 2015, 455-464, doi: 10.1016/j.ijheatmasstransfer.2015.03.030.
- [28] Bordbar, A., Kamali, R., Taassob, A., Thermal performance analysis of slug flow in square microchannels, *Heat Transfer Engineering*, 41(1), 2020, 84-100, doi: 10.1080/01457632.2018.1513630.
- [29] Vivekanand, S.V.B., Raju, V.R.K., Numerical study of the hydrodynamics and heat transfer characteristics of liquid-liquid Taylor flow in microchannel, *Heat Transfer—Asian Research*, 47(6), 2018, 794-805, doi: 10.1002/htj.21341.
- [30] Chandrasekhar, S., Raju, V.R.K., Two-phase flow and heat transfer through wavy microchannel, 2020, 59-65, [Online]. Available: <https://www.theijes.com/papers/NHTFF-2020/Volume -2/10, 59-65.pdf>.
- [31] Li, X., He, L., Qian, P., Huang, Z., Luo, C., Liu, M., Heat transfer enhancement of droplet two-phase flow in cylindrical microchannel, *Applied Thermal Engineering*, 186, 2021, 116474, doi: 10.1016/j.applthermaleng.2020.116474.
- [32] Chandrasekhar, S., Raju, V.R.K., Boundary Condition Effect on Two-Phase Fluid Flow and Heat Transfer inside 3-D Microchannels, *Journal of Applied Fluid Mechanics*, 14(6), 2021, 1755-1765, doi: 10.47176/jafm.14.06.32493.
- [33] Hirt, C.W., Nichols, B.D., Volume of fluid (VOF) method for the dynamics of free boundaries, *Journal of Computational Physics*, 39(1), 1981, 201-225, doi: 10.1016/0021-9991(81)90145-5.
- [34] Asadolahi, A.N., Gupta, R., Fletcher, D.F., Haynes, B.S., CFD approaches for the simulation of hydrodynamics and heat transfer in Taylor flow, *Chemical Engineering Science*, 66(22), 2011, 5575-5584, doi: 10.1016/j.ces.2011.07.047.
- [35] Khan, W., Chandra, A.K., Kishor, K., Sachan, S., Alam, M.S., Slug formation mechanism for air-water system in T-junction microchannel: a numerical investigation, *Chemical Papers*, 72, 2018, 2921-2932, doi: 10.1007/s11696-018-0522-7.
- [36] Brackbill, J.U., Kothe, D.B., Zemach, C., A continuum method for modeling surface tension, *Journal of Computational Physics*, 100(2), 1992, 335-354, doi: 10.1016/0021-9991(92)90240-Y.
- [37] Murshed, S.S., De Castro, C.N., A critical review of traditional and emerging techniques and fluids for electronics cooling, *Renewable and Sustainable Energy Reviews*, 78, 2017, 821-833, doi: 10.1016/j.rser.2017.04.112.
- [38] Sekrani, G., Poncet, S., Ethylene-and propylene-glycol based nanofluids: a literature review on their thermophysical properties and thermal performances, *Applied Sciences*, 8(11), 2018, 2311, doi: 10.3390/app8112311.
- [39] Cas, N., Information en matière de sécurité donnée volontairement au sens du formulaire FDS conformément au Règlement (CE) N ° 1907 / 2006 (REACH) RUBRIQUE 1 : Identification de la substance / du mélange et de la société / l ' entreprise Information en matière, 2006, 2021, 1-14.
- [40] Said, M., Nait Bouda, N., Harmand, S., Numerical Investigation of Flow Patterns and Plug Hydrodynamics in a 3D T-junction Microchannel, *Microgravity Science and Technology*, 35(1), 2023, 8, doi: 10.1007/s12217-022-10026-9.
- [41] Dombrowski, N., Fomeny, E.A., Ookawara, S., Riza, A., The influence of Reynolds number on the entry length and pressure drop for laminar pipe flow, *The Canadian Journal of Chemical Engineering*, 71(3), 1993, 472-476, doi: 10.1002/cjce.5450710320.
- [42] Gupta, R., Fletcher, D.F., Haynes, B.S., On the CFD modelling of Taylor flow in microchannels. *Chemical Engineering Science*, 64(12), 2009, 2941-2950, doi: 10.1016/j.ces.2009.03.018.
- [43] ANSYS, ANSYS FLUENT User's Guide, vol. 15317, no. October. 2012.
- [44] Yao, C., Zheng, J., Zhao, Y., Zhang, Q., Chen, G., Characteristics of gas-liquid Taylor flow with different liquid viscosities in a rectangular microchannel, *Chemical Engineering Journal*, 373, 2019, 437-445, doi: 10.1016/j.cej.2019.05.051.
- [45] Kreutzer, M.T., Kapteijn, F., Moulijn, J.A., Heiszwolf, J.J., Multiphase monolith reactors: chemical reaction engineering of segmented flow in microchannels, *Chemical Engineering Science*, 60(22), 2005, 5895-5916, doi: 10.1016/j.ces.2005.03.022.
- [46] Walsh, P.A., Walsh, E.J., Muzychka, Y.S., Heat transfer model for gas-liquid slug flows under constant flux, *International Journal of Heat and Mass Transfer*, 53(15-16), 2010, 3193-3201, doi: 10.1016/j.ijheatmasstransfer.2010.03.007.
- [47] Che, Z., Wong, T.N., Nguyen, N.T., Heat transfer enhancement by recirculating flow within liquid plugs in microchannels, *International Journal of Heat and Mass Transfer*, 55(7-8), 2012, 1947-1956, doi: 10.1016/j.ijheatmasstransfer.2011.11.050.
- [48] Muzychka, Y.S., Walsh, E., Walsh, P., Simple models for laminar thermally developing slug flow in noncircular ducts and channels, *Journal of Heat Transfer*, 132, 2010, doi: 10.1115/1.4002095.
- [49] Abadie, T., Xuereb, C., Legendre, D., Aubin, J., Mixing and recirculation characteristics of gas-liquid Taylor flow in microreactors, *Chemical Engineering Research and Design*, 91(11), 2013 2225-2234, doi: 10.1016/j.cherd.2013.03.003.
- [50] Talimi, V., Muzychka, Y.S., Kocabiyyik, S., Effects of film thickness on heat transfer in Taylor flows under constant wall heat flux boundary condition, *ASME International Mechanical Engineering Congress and Exposition*, 45233, 2012, 2033-2040, doi: 10.1115/IMECE2012-86123.
- [51] Sawicka, D., Cieśliński, J.T., Smolen, S., A comparison of empirical correlations of viscosity and thermal conductivity of water-ethylene glycol-Al2O3 nanofluids, *Nanomaterials*, 10(8), 2020, 1487, doi: 10.3390/nano10081487.
- [52] Sagdeev, D.I., Fomina, M.G., Abdulgatov, I.M., Density and viscosity of propylene glycol at high temperatures and high pressures, *Fluid Phase Equilibria*, 450, 2017, 99-111, doi: 10.1016/j.fluid.2017.07.006.
- [53] Maranzana, G., Perry, I., Maillet, D., Mini-and micro-channels: influence of axial conduction in the walls, *International Journal of Heat and Mass Transfer*, 47(17-18), 2004, 3993-4004, doi: 10.1016/j.ijheatmasstransfer.2004.04.016.
- [54] Mehta, B., Khandekar, S., Measurement of local heat transfer coefficient during gas-liquid Taylor bubble train flow by infra-red thermography, *International Journal of Heat and Fluid Flow*, 45, 2014, 41-52, doi: 10.1016/j.ijheatfluidflow.2013.12.001.



ORCID iD

M. Said  <https://orcid.org/0000-0002-4897-6382>

N. Nait Bouda  <https://orcid.org/0009-0005-3643-1122>

S. Harmand  <https://orcid.org/0009-0003-5812-5041>



© 2023 Shahid Chamran University of Ahvaz, Ahvaz, Iran. This article is an open access article distributed under the terms and conditions of the Creative Commons Attribution-NonCommercial 4.0 International (CC BY-NC 4.0 license) (<http://creativecommons.org/licenses/by-nc/4.0/>).

How to cite this article: Said M., Nait Bouda N., Harmand S. 3D Numerical Investigation of Heat Transfer Performance in Liquid-liquid Taylor Flow, *J. Appl. Comput. Mech.*, 10(1), 2024, 183–204. <https://doi.org/10.22055/jacm.2023.44421.4211>

Publisher's Note Shahid Chamran University of Ahvaz remains neutral with regard to jurisdictional claims in published maps and institutional affiliations.

